Title
Simulating the Effects of Surface Energy Partitioning on Convective Organization: Case Study and Observations in the US Southern Great Plains

Journal
Journal of Geophysical Research: Atmospheres, 126(2)

ISSN
2169-897X

Authors
Dai, Y
Williams, IN
Qiu, S

Publication Date
2021-01-27

DOI
10.1029/2020JD033821

Peer reviewed

Simulating the effects of surface energy partitioning on convective organization: Case study and observations in the US Southern Great Plains

Yi Dai[1], Ian N. Williams[1,2], and Shaoyue Qiu[1]

1 Climate and Ecosystem Sciences Division, Lawrence Berkeley National Laboratory, Berkeley, CA, USA

2 Department of Geological and Atmospheric Sciences, Iowa State University

Corresponding author: Yi Dai (yidai@lbl.gov)

Key points

- Wet soil can lead to better organized convection than dry, constituting a positive rainfall feedback, despite earlier triggering over dry
- Cold pools diminish or contribute to feedback; their effects vary with convective lifecycle stage and are not captured in parameterizations
- Enhanced surface latent heat flux along gust fronts provides additional positive feedback that may help convection persist after sunset

Abstract

Realistic cloud-resolving simulations were performed to study the effects of surface energy partitioning (surface sensible and latent heat fluxes) on the organization of isolated convection into larger mesoscale convective systems (MCSs) near the US Southern Great Plains. The role of cold pools in mediating surface-convection interactions was explored. Better organized MCSs tended to occur in the experiments with perturbed wetter soil (and more active vegetation), regardless of the effects of soil moisture on the diurnal timing of convective triggering. Wetter soil led to shallower boundary layers and more convective available potential energy than drier soil. The roles of cold pools on convection are lifecycle-stage dependent: A dry surface allows more numerous colliding cold pools, thereby aiding in convective triggering by reducing entrainment in the early stages, and providing gust-front uplift in later stages. However, horizontal propagation of the cold-pool density current can outrun the convective system, creating a slantwise updraft and thus weakening the gust front uplift in later stages. This effect calls into question previous cold pool parameterizations, in which the gust front uplift is mainly proportional to the negative buoyancy of cold air. Lastly, both the model and observation show an enhancement of surface latent heat flux during the passage of a gust front at night, suggesting that a positive feedback between the surface and convection helps MCSs to persist into the nighttime.

Plain Language Summary

Numerical simulations explicitly resolving thunderstorms were used to study the effects of the land surface (soil moisture/vegetation) on rainfall in the US South Great Plains. Better convective organization (larger, stronger thunderstorm clusters with heavier rainfall) occurred more often in perturbed wetter soil/vegetation experiments than in dry experiments, indicating a positive feedback of soil moisture on rainfall. A case study was conducted to explore the mechanism of this feedback. Although dry soil is initially more favorable for triggering thunderstorms, wetter soil can modify environmental conditions (convective available potential energy) to become more favorable for further development of isolated thunderstorms into larger organized clusters. Current climate models do not fully capture the feedback mechanisms indicated here. The results provide insight into how climate models can be improved to more realistically represent processes connecting rainfall to future land-surface change.

1. Introduction

Evapotranspiration not only directly provides water vapor for precipitation, it also influences convective precipitation by changing atmospheric dynamics and stability (Schar et al., 1999). The interaction of convection with the land surface is complicated because it depends on the lifecycle stage of convective precipitation—isolated convective cells are initially triggered, but can grow upscale into organized clusters. Atmospheric state-dependence, spatial heterogeneities in soil and vegetation, and spatial and temporal scale dependence (Guillod et al. 2015) add further complexity. For example, modeling (e.g., Findell & Eltahir 2003a; Williams, 2019; Konings et al., 2010; Gentine et al., 2013; Yin et al., 2015) and observational studies (Qiu and Williams, 2020) have shown that whether a wet or dry surface is more favorable for triggering convection depends mainly on the early-morning low-level temperature (stratification) and humidity structure. Specifically, convection is more easily triggered over dry soil and heat surface sensible heating, when the rapidly growing planetary boundary layer (PBL) overcompensates the increase of the level of free convection (LFC) due to a drier atmosphere, causing a negative feedback. Yet the sign of the feedback on precipitation may change from negative to positive after convection is triggered and organized (e.g., Gantner & Kalthoff, 2010; Froidevaux et al., 2014).

Convective organization is an important process in the water cycle, because once convective cells are organized, the system is more likely to persist and produce more rainfall. Organized convective clouds are often referred to as mesoscale convective systems (MCSs) when their precipitation region exceeds 10,000 km^2, or is over 100 km in at least one dimension (Houze 2004). MCSs are a major source of summertime extreme weather and precipitation in continental climates (Fritsch et al., 1986; Feng et al., 2016), including over the US Southern Great Plains (SGP) where our study is based. The failure of climate models in capturing convective organization contributes to the erroneous diurnal timing of summer precipitation and covnective clouds over land at midday instead of the observed late afternoon and night (e.g., Dai et al., 1999; Yang & Slingo, 2001; Pfeifroth et al., 2012; Yin et al., 2020).

Cloud-resolving models can simulate a positive feedback of soil moisture on convection in the mature stage of organized convective systems in real-case studies (e.g., over West Africa; Gantner & Kalthoff, 2010). Whether such feedbacks work in other environments, and by what mechanisms, are fundamental questions for reducing uncertainties in drought and heavy precipitation projections (e.g., Zeng et al., 2019). Findell and Eltahir (2003a) did not address the question of convective organization as their boundary layer model was switched off as soon as convection was triggered. Schar et al. (1999) found more precipitation in perturbed wet soil experiments in a regional climate model with convective parameterization, primarily because the wet soils led to a shallower boundary layer and a build-up of convective available potential energy (CAPE). Hohenegger et al. (2009) found a different result from Schar et al. (1999): in the coarse-resolution climate model, the results were similar to Schar et al. (1999), in that wet soils ensure more precipitation; however, in the cloud-resolving model, the dry soil led to more precipitation. Although a particular condition (a stable layer on top of the PBL) exists in Hohenegger et al. (2009), the spatial resolution is no doubt a key difference. Therefore, in this paper we use a cloud resolving model to explore land-surface feedback on convective organization.

A major advantage of cloud-resolving models is their ability to resolve the convection-coupled cold pool which results from the combination of cooling by evaporation of precipitation, the downward drag effect of falling hydrometers, and downward dynamic pressure gradient force in convective updrafts. Cold pools are thought to play important roles in convective organization. The cold pool can thermodynamically support new convection by creating cold and moist air within the edge of the cold pool (e.g., Tompkins, 2001; Torri et al., 2015). The CAPE is increased and the convective inhibition (CIN) is decreased along the edge of the cold pool. Another mechanism is the ascent within the narrow surface gust front zone caused by convergence of the cold-pool air and environmental air (e.g., Rotunno et al., 1988; Jeevanjee & Romps, 2015; Torri et al., 2015). By creating larger convergence near the gust fronts, cold pools whose propagation and strength are dynamically balanced with environmental shear might aid in organizing convection (Rotunno et al., 1988). Moreover, colliding cold pools help create larger clouds (Feng et al., 2015; Haerter et al., 2019), which have lower entrainment rates than smaller clouds (e.g., Kuang & Bretherton, 2005; Khairoutdinov & Randall, 2006; Schlemmer & Hohenegger, 2014), favoring stronger convection. Stronger convection might in turn create stronger gust fronts, and a positive feedback on convective organization.

The cold pool could be a natural agent in connecting the land surface with convective organization. Hypothesized mechanisms for this connection can be grouped into three broad categories, involving cloud entrainment, stability (CAPE), and surface flux interactions. First, cold pool dynamics could link the convective triggering feedback and convective organization via cloud entrainment. For example, a drier surface could produce deeper boundary layers, triggering more numerous isolated convective cells and thus more intersecting cold pools than a wetter surface; leading to wider convective clouds, reduced entrainment, and better convective organization. On the other hand, over wet soils where shallow boundary layers can accumulate CAPE, convergence along gust fronts could provide a mechanism to lift the unstable air to the LFC (Froidevaux et al., 2014), producing a positive soil moisture-precipitation feedback analogous to that in climate models which lack cold pool dynamics (Schar et al., 1999). Those models parameterized convection as a function of CAPE, and thus may correctly capture the soil moisture-CAPE relationship in some cases for the wrong physical reason (e.g., Hohenegger et al. 2009), which warrants further study here. Lastly, when the cold and unsaturated downdraft air in the cold pools contacts the surface, both the surface sensible and latent heat fluxes will change due to the temperature and moisture difference between the land surface and near-surface atmosphere, as well as due to the increased wind speed associated with the gust fronts. If the location of the enhanced surface fluxes is close to the location of the newly triggered convection (near the gust front), we can expect that organized convection will persist into the nighttime.

Adding cold pool parameterizations to climate models has led to improved convective precipitation over land (Rio et al., 2009; Grandpeix & Lafore, 2010) and ocean (Del Genio et al., 2015), in terms of the diurnal cycle and amount. However, potential interactions of cold pools with the land-surface, noted above, are not yet taken into account. Moreover, these interactions have been investigated mainly in idealized small-domain cloud resolving models or large eddy simulations (LESs), without resolving the full spatial scale of realistic organized convective systems or MCSs. The motivation of this paper is threefold. First, we want to investigate how land surface fluxes affect the convective organization in real case experiments using a cloud resolving model. Second, we want to test hypothesized cold pool effects on convective organization as suggested by smaller-domain studies. Finally, we are hoping to have some insights into the cold pool and convective parameterizations for global models.

2. Methodology

2.1. Model description

The Weather Research and Forecasting (WRF, version 3.8.1, Skamarock et al., 2008) model was used to simulate realistic MCSs near the SGP site. The simulated domain contained 454 x 600 grid points with horizontal grid spacing of 3 km, over a region from about 28° N 42° N meridionally, and 105° W to 92° W zonally. Vertically, layer thickness gradually increased from about 50 m near the surface to 400 m at z = 2500 m, and was constant at about 750 m upward to the model top at around 20,000 m. The 6-h North American Mesoscale Forecast System (NAM, 12-km horizontal resolution, available from March 2004 to present) was used for both the initial condition and lateral boundary condition.

Table 1 shows the model physics schemes used in this study. No cumulus scheme was used because the 3-km horizontal resolution is able to resolve clouds. The RRTMG scheme (Iacono et al., 2008) was used for both shortwave and longwave radiation. We have chosen the Thompson scheme (Thompson et al., 2008) for microphysics, because comparison of different microphysics schemes in test experiments (not shown) indicated that the Thompson scheme was better to represent the MCS cloud field than other schemes. The MYNN level 2.5 scheme (Nakanishi & Niino, 2009) was used for the planetary boundary layer.

The Community Land Model Version 4 (CLM4, Lawrence et al., 2011) was used for land surface parameterization, with modifications described below. Although newer versions of CLM are available, CLM4 was the latest supported version coupled to WRF (Lu & Kueppers, 2012) at the start of our study. For this study, modifications were made to CLM4 in WRF to better represent the land surface in the Southern Great Plains (as described in Williams et al. 2020). Notably, stomatal and soil resistance parameters were changed to better represent surface energy partitioning compared to observations, and higher-resolution input soil and vegetation datasets were used. The latter include a new plant functional type and leaf area index dataset developed to capture the heterogeneous distribution of winter crops and grasses across much of Oklahoma and Kansas. WRF-CLM was initialized with a spun-up offline run of CLM forced with meteorological data including 4 km gridded hourly precipitation data combining WSR-88D NEXRAD radar and rain gauge estimates (see Williams et al. 2020).

Table 1. Model physics schemes used in this study

WRF physics schemes	
Radiation (longwave and shortwave)	RRTMG (Iacono et al., 2008)
Microphysics	Thompson scheme (Thompson et al. 2008)
PBL	MYNN level-2.5 (Nakanishi & Niino, 2009)
Land surface model	CLM4 (Lawrence et al. 2011)

2.2. Study site and selection of MCS cases

MCSs can originate as surface-based isolated convective clouds (cumulonimbus), which often organize over the US High Plains and propagate over the SGP at night in concert with the nocturnal low-level jet. However, it is not unusual for MCSs to develop from isolated convection over the SGP as well. Of these, we are particularly interested in cases of weak synoptic forcing, in which the land surface could have greater influence. Weakly forced cases are also of interest as they pose a greater challenge for numerical forecast models (Squitieri and Gallus, 2016). We focused on events triggered near the US Department of Energy Atmospheric Radiation Measurement (ARM) site, which includes a dense network of surface and atmospheric profiling measurements over Northern and Central Oklahoma and Southern Kansas. The long-term operation of this network from approximately 1999 to present allowed several cases to be selected in contrasting environments, as described below.

We used the Geostationary Operational Environmental Satellite (GOES, Minnis et al. 2008) data (4 km spatial resolution and 30-minute temporal resolution) to identify events in which afternoon (12:00-18:00 LST) convection is triggered and subsequently organized near the SGP site. Details are provided in Qiu and Williams (2020) and briefly summarized here. A cloud system was defined by contiguous cloudy pixels in the GOES visible cloud mask data. Events that were initiated from isolated cumulonimbus were separated from propagating events initiated outside the SGP region, based on size and time evolution (events were required to start as isolated deep cumulus and grow in excess of 100 km x 100 km). From this larger sample, we removed cases by visual inspection that were associated with strong frontal boundaries (to focus on surface influences) and removed cases that did not have contiguous precipitation extending over 100 km in at least one direction (using the Next Generation Weather Radar [NEXRAD] reflectivity). Note that our selection of MCSs included both cases that are organized into compact clusters with strong convective cells, and those that cover a large region but with relatively weak and scattered multicellular cells (to be shown in Fig. 1 and Fig. S1, S2).

To further narrow the cases a computationally feasible sample size most relevant to our hypotheses (three mechanisms in the Introduction), we chose cases in the wettest and driest quartiles of morning (09:00-12:00 LST) surface evaporative fraction (defined as the ratio of latent heat flux to the sum of latent and sensible heat flux) over a 3° x 3° domain centered over the ARM Central Facility, based on surface flux measurements (Tang et al. 2019). The evaporative fraction was used because latent heat and sensible fluxes can also be influenced by net radiation. Of the drier cases, we required that the morning (07:00 LST) lower-tropospheric relative humidity and thermal stratification be in the negative 'triggering feedback' regime or so-called 'dry-soil-advantage' regime as defined earlier (e.g., Qiu and Williams, 2020; Williams, 2019; Findell and Eltahir, 2003a), and likewise for the wettest quartile we selected those in the positive triggering feedback regime. As noted in the introduction, over a land surface with low evaporative fraction (high sensible heating) and in tropospheric states where the rapidly growing planetary boundary layer (PBL) can overcompensate for the increase of the LFC due to a drier PBL, a negative 'triggering feedback' on convective triggering occurs; i.e., negative soil moisture anomalies are more likely to trigger deep convection. On the other hand, a positive feedback is hypothesized when moistening of the low-level atmosphere brings the LFC down to the PBL top, preferentially triggering convection over wet soil or actively transpiring vegetation. While regime-based selection does not guarantee cases in which MCS development will exhibit sensitivity to surface forcing, it provides a practical starting point for case selection given the computational infeasibility of simulating all MCS cases.

A total of 14 cases (9 in negative feedback regime and 5 in the positive regime) were chosen and simulated. Dates for negative regime cases were 2006-08-10, 2011-07-02, 2011-07-12, 2011-07-24, 2011-08-06, 2011-08-24, 2012-05-29, and 2012-07-19. Dates for the positive regime were 2007-06-19, 2007-07-04, 2007-07-14, 2015-07-20, and 2007-08-02. After exploring common features across cases, we focused on one typical case to test the detailed hypotheses noted above, and to allow for additional experiments on the role of cold pools.

2.3. Perturbed WET and DRY surface condition

The effect of surface energy partitioning in this paper is realized by perturbing the soil moisture. As described above, a spun-up offline run of CLM was used to provide land surface initial conditions for WRF in which soil moisture reflects observed meteorological forcing and thus represents real hindcast days. We hereafter refer to these simulations as the 'control' or CTL. To explore the impacts of the hydrologic state of the land surface on convective organization, two additional experiments were performed in which soil moisture was initialized higher and lower than the reference (WET and DRY experiments, respectively). The perturbed high and low values were defined by the maximum and minimum values of the model daily summer (June-August) climatology (2000-2016), defined per grid cell and soil vertical level. These perturbations are plausible yet large enough for exploring the general effect of wet versus dry surface conditions on convection (e.g., as opposed intraseasonal variability in monthly soil moisture anomalies from climatology; Koster et al. 2003). In CLM4, the soil solumn is 42 m deep, but for grasses and C3 crops about 90% of the root fraction is in the top 0.83 m of the soil column, which can be considered the relevant 'surface' soil depth with respect to evapotranspiration from a vegetated surface. The upper 10 layers received the soil moisture perturbation, with the top layer between 0-1.8 cm, and bottom layer between 229.6-380.2 cm (Lawrence et al. 2011).

Our experiments were designed to explore the response of convection to relatively homogeneously dry or wet surface conditions in which the convective boundary layer is deep or shallow over a large area. The area of the soil moisture perturbation was confined to a circle of diameter 500 km (on the order of the internal Rossby radius of deformation), centered over the SGP site. To avoid a sharp discontinuity in soil moisture, perturbations were tapered to 0 linearly over an extended region 350 km outward from the edge of the circular perturbation. With this smooth gradation in soil moisture, we did not observe gravity waves or secondary circulations associated with the edge of the perturbed region. Note that our deliberate focus on large-scale anomalies in surface energy partitioning (as opposed to smaller mesoscale heterogeneity or landscape 'patchiness') is motivated by the fact that many convective parameterizations (with CAPE-based trigger functions) still do not realistically couple convective triggering to boundary layer turbulence, which can provide a lifting mechanism to overcome convective inhibition energy regardless of whether the turbulence is driven by a horizontally homogeneous or heterogeneous surface (e.g., Williams, 2019). Moreover, such large-scale soil moisture (and vegetation state) anomalies are common during major droughts and pluvial events.

Our intent in performing the WET and DRY experiments is not to quantify soil moisture effects per se, but to explore how convection responds to variations in surface evaporative fraction. To achieve this goal, it is necessary to consider the physical properties of soil and vegetation that may limit evapotranspiration even if the soil column is near saturation. For this reason, our WET configuration was additionally modified to have reduced stomatal and soil resistances to evapotranspiration. Specifically, we reduced the leaf-litter layer resistance by a factor 0.5, and increased the stomatal conductance by a factor of 2. The latter helped raise the upper limit on transpiration that is imposed by model vegetation, and was implemented after initial tests revealed vegetated areas with muted responses of latent heat flux when WET was configured using soil moisture perturbations alone. The result of these modifications is that WET represents a land surface with actively transpiring vegetation, ample soil moisture supply, and reduced leaf-litter impedance of bare soil evaporation. The comparison of simulations before and after the stomatal and soil resistance modifications are shown in Fig. S1c. Overall, these modifications help to create a larger difference between DRY and WET simulations.

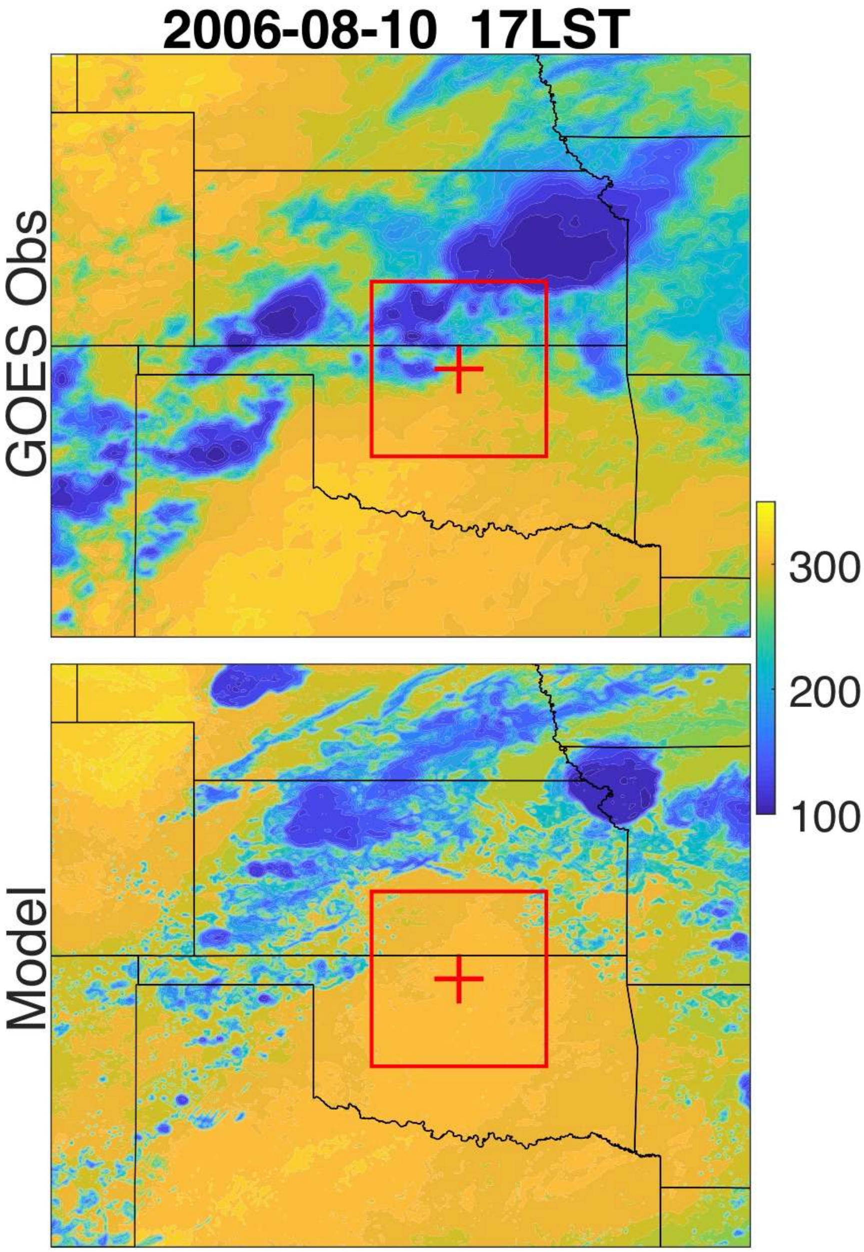

Figure 1. Comparison of OLR (W/m2) between the GOES observation (upper panel) and model data (lower panel), for case 2006-08-10 at 17:00 LST near the SGP site (red cross: 36.6 N, 97.5 S). Red box indicates 3^o X 3^o domain centered at the SGP site.

3. General behavior of simulations

3.1. Validity of simulated MCSs

We first verified how well the chosen cases are captured by control (CNT) simulations. Snapshots of the outgoing longwave radiation (OLR) for both the simulations and the Geostationary Operational Environmental Satellite (GOES) data are used to compare case 2006-08-10 in Fig. 1. The comparisons of all the other 13 cases are shown in Fig. S1 and S2. The model seems to show smaller convective-scale features, compared to the observation. Overall, the model is quite good at capturing the observed deep convective cloud field, although some spatial and temporal displacements exist. In a few cases, such as 2011-07-30, 2007-08-02, and

2007-06-19, parts of the convective feature are not simulated; also, case 2007-06-19 has a lagged (about 3 hours) convective response in the model compared to observation. We choose to keep those cases, because model sensitivity to soil moisture (which is the main focus of this paper) in those cases is large. The difference between model and observations in those cases also indicates the difficulty in simulating the weakly forced MCSs. We note that initial condition sensitivity tests (varying the model initialization time between 00:00, 06:00, and 12:00 UTC) did not significantly change the location and timing of convection, and for brevity we discuss results initialized at 06:00 UTC.

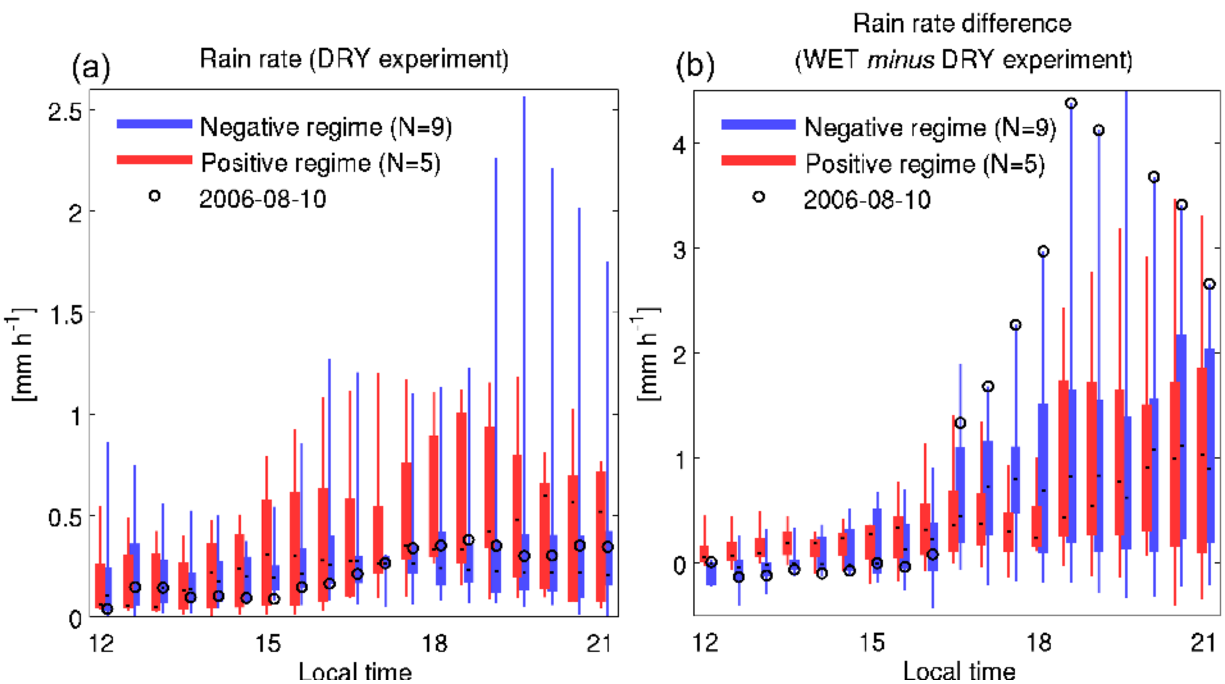

Figure 2. Half-hourly rain rate (spatial average, 600km X 600km centered at SGP site) for cases in positive (red) and negative (blue) triggering feedback regimes. Black notches, shaded bars, and lines indicate the median, interquartile range, and extrema, respectively. Positive and negative regime results are slightly offset to aid visualization.

3.2. WET *VS* DRY simulations

Next, we compared the increased soil moisture (WET) and decreased soil moisture (DRY) experiments. Fig. 2 shows the time series of the area-mean rain rate for DRY (Fig. 2a) and the difference between WET and DRY (Fig. 2b), in a statistical way for all the negative and positive regime cases. To be consistent with the criterion used in choosing cases, we chose the area that is centered in the SGP site, with a size of 600 km by 600 km in order to include MCSs that might have some location difference from observed ones. In DRY experiments (Fig. 2a), late afternoon and early evening (around 16:00-20:00 LST) have slight preference for higher rain rates than other times, although large variations exist across simulations. Overall, rain rate is low for all cases in DRY simulations. In contrast, WET simulations generally have a higher rain rate than DRY regardless of triggering feedback regime (note that y-axis scale in Fig. 2b is larger than Fig. 2a). For most negative regime cases, rain rate in WET is slightly weaker than DRY before about 16:00 LST; for positive regime cases rain rate in WET is much higher than DRY before 16:00 LST, consistent with the regime-dependent triggering feedback hypothesis discussed above (dry soil is more favorable for triggering convection in the negative regime). However, later on, much larger rain rate occurs in WET compared to DRY even in negative regime cases, and this trend persists until the end of simulations. For positive regime cases, WET always has a larger rain rate than DRY for the whole time period. The takeaway message in Fig. 2 is that, in most simulated cases, WET has a larger rainfall rate than DRY in the late afternoon or early evening (although large variation exists across simulations), regardless of the initial influence of the surface perturbation on triggering. It is noteworthy that not every case shows such a feature. In the negative regime case of 2011-08-24, the WET experiment has almost no rain or convection during the whole simulation, due to a very stable boundary layer that does not allow convection to initiate over the wetter surface. We conclude that while evapotranspiration can sometimes determine whether organized convection develops at all, in most of our cases the influence of the surface on triggering is dominated by its positive influence on the later stages of organization.

4. 2006-08-10 case

4.1 Gust fronts and convective cells

We chose the 2006-08-10 case (black circles in Fig. 2) to evaluate in detail the three mechanistic hypotheses of cold pool-mediated surface influences on convective organization described in the introduction (involving surface fluxes, CAPE, and cloud entrainment). To do so we compared the behavior of cold pools, gust fronts, and cloud cell size between WET and DRY. Compared with other cases, 2006-08-10 is representative of a fairly typical case that is neither extraordinarily strong, nor in a particularly favorable environment (with a moderate CAPE of about 1000 J/kg). However, it also exhibits the switch in feedback suggested in earlier studies, from an initially negative triggering feedback to a positive feedback on rain rate at the mature stage. In particular, we focus on understanding the much greater mature-stage rain rate in WET despite earlier triggering in DRY. Before presenting the detailed results, we first present the surface energy partitioning for 2006-08-10 CTL, DRY, and WET, respectively in Figure S1. Evaporative fraction (EF) is used to show the surface energy partitioning. EF does not change much from morning to mid-afternoon (Fig. S1a): in both of CTL and DRY, EF is small at around 0.2 (with slight larger value in CTL), indicating that the sensible heating is leading the surface fluxes. On the contrary, EF in WET is close to 1, meaning that the latent heating is much larger than sensible heating.

Gust fronts are the enhanced near-surface wind created by cold pool downdrafts. They are located near the edge of cold pools where low-level wind and density show discontinuity. Based on air continuity, gust fronts in this paper are visualized by positive vertical velocity in the lower boundary layer. A comparison of boundary layer gust fronts between DRY and WET experiments (Fig. 3) shows that numerous small convection-induced gust fronts exist early in the convective triggering stage at 14:00 LST in DRY (Fig. 3a), while there are almost no gust fronts in WET at that time (Fig. 3d). As stated above, the 2006-08-10 case falls within the negative (dry advantage) regime, in which convective triggering is hypothesized to occur more readily over a drier surface having higher sensible heat flux (SH). Indeed, these results suggest more numerous colliding gust fronts and a possible pathway for a dry surface to influence convective organization in favorable environments. Note that the line-type positive and negative vertical velocities prevalent in Fig. 3a are convective rolls driven by turbulence in the planetary boundary layer. In DRY, sensible heating is much higher than WET in the afternoon, creating a very active turbulent boundary layer. This feature nearly occurs in every DRY simulation, and it is not sensitive to planetary boundary layer parameterizations (results not shown in figures).

Careful inspection of Fig. 3 suggests that the strong and deep convective cells (black contours in Fig. 3 indicate vertical velocity = 2 m/s at z = 6 km) are mainly located in the centers of cold pool downdrafts, while new small cells are located at gust fronts where cold pools collide (Fig. 3a). This behavior is consistent with the fact that cold pools are a consequence of precipitating deep convection, and suggests that colliding cold pools are effective in triggering new convection (e.g., Schlemmer and Hohenegger 2014; Feng et al. 2015; Haerter et al. 2019). However, the earlier triggering of convection and colliding cold pools in DRY does not ensure a stronger or more organized MCS at later stages. Instead, we see a better organized and longer-lasting MCS in WET (Fig. 3c vs. Fig. 3f). Looking at the time evolution of convection in DRY (Fig. 3a-c), the area with active convection is getting smaller throughout the afternoon and evening. While gust fronts still exist in the later stage (Fig. 3c), most of them barely collocate with deep convection. On the contrary, although deep convective cells are triggered at a later time in WET than DRY, they eventually become better organized and stronger with time (Fig. 3d-f). Therefore, our simulations show the importance of surface energy partitioning for MCS development, and that colliding cold pools alone are not sufficient to develop or sustain an MCS when the environment is unfavorable.

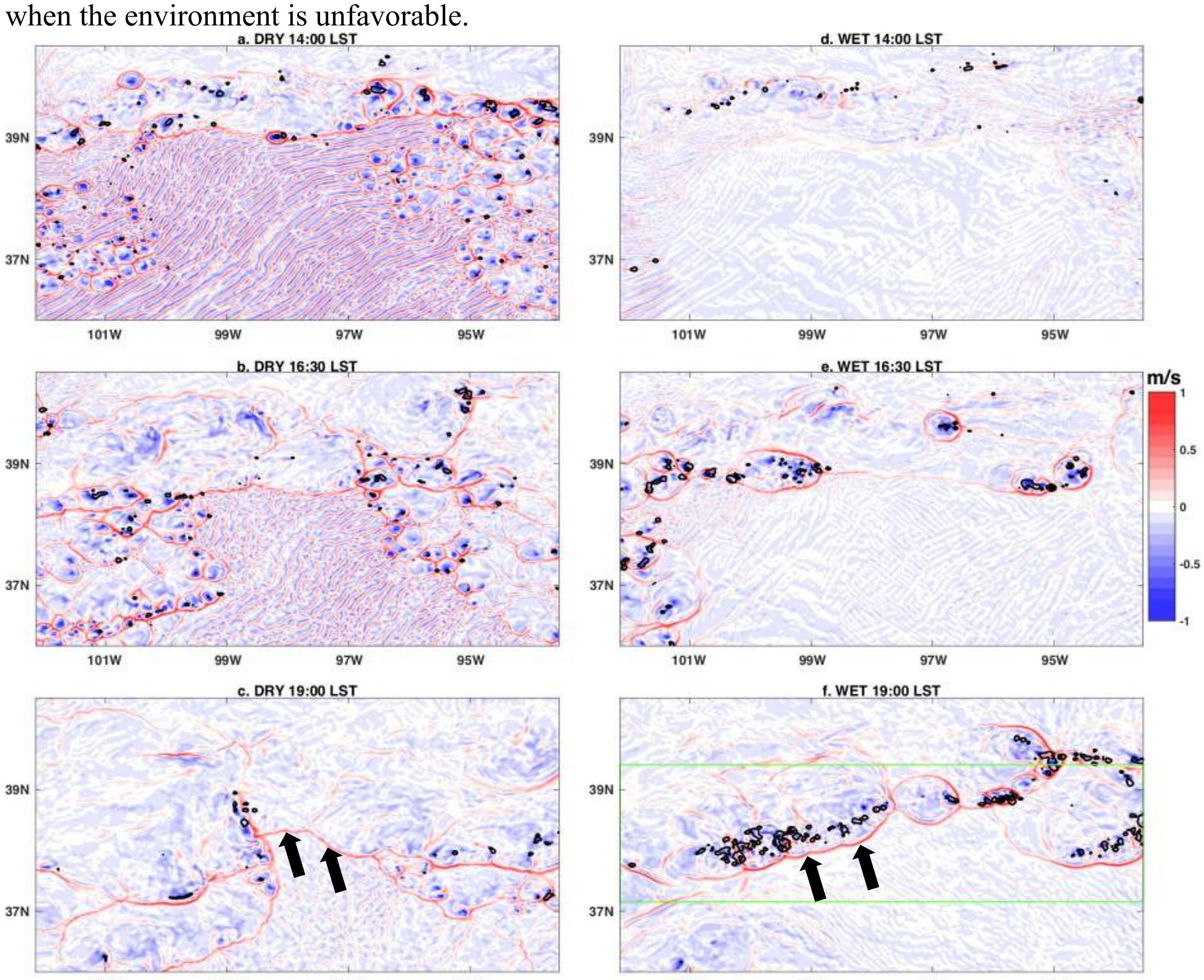

Figure 3. Time evolution of DRY (left panels) and WET (right panels) experiments for 2006-08-10 case. Shading is vertical velocity (m/s) at z = 200 m, and black contours indicate vertical velocity of 2 m/s at z = 6 km. The green box in f indicates the region used for moist static energy analyses shown below. Black arrows in c and f are examples of locations of gust fronts.

4.1.1. MSE analysis

To address both the CAPE and entrainment mechanisms noted in the introduction, we analyzed the moist static energy (MSE). Specifically, we hypothesized that the shallower PBL over the wetter surface allowed MSE to accumulate in the PBL, providing more CAPE for mesoscale circulations at later stages in WET (as in Schar et al. 1999). Fig. 4 shows the probability density function (PDF) of the frozen MSE, which is defined as $MSE = C_pT + gz + L_vq_v - L_fq_i$, where C_p is the dry air specific heat, T the temperature, L_v and L_f the latent heat of vaporization and freezing, and q_v and q_i the specific humidities of water vapor and ice. The MSE is then divided by C_p to have a temperature (K) unit. We use the frozen MSE because it is nearly conserved even with the presence of ice phase change. We have chosen a relatively narrow subdomain (magenta box in Fig. 3f) in order to minimize the effects of meridional temperature gradient. The chosen subdomain contains most of the MCS as well as the environment.

Similar to Schar et al. (1999), the cooler surface in WET (energy is used to evaporate water instead of heating the surface) makes a shallower boundary layer and less entrainment mixing with the overlying atmosphere than DRY. This effect concentrates more MSE near the surface, creating a sharper gradient in MSE across the PBL top in WET (lower panels of Fig.4) compared to DRY (upper panels of Fig. 4), indicating larger CAPE in WET than in DRY. This is partly due to less PBL-entrainment and mixing of surface enthalpy fluxes with the more stable air above the PBL; but also the higher boundary layer q_v and lower air temperature by the wetter soil moisture reduces the difference between the dewpoint and temperature (increased relative humidity, not shown) in the boundary layer, causing a much lower LCL and LFC in WET than DRY (the starting point of the entraining plume model to be shown below indicates the height of LCL). At 14:00 LST, the area-mean (within the magenta box in Fig. 3f) CAPE in WET is about 4000 J/kg, while it is only about 500 J/kg in DRY. As a result, both the time evolution of MSE (Fig. 4) and vertical mass flux (Fig. 5) indicate that WET has stronger convective organization than DRY at later stages.

As an aside, it is worth noting that the vertical integral of MSE is slightly greater in WET (not shown), so that weaker vertical exchange across the PBL is not the only factor in explaining the higher near-surface MSE in WET. The change in energy partitioning from sensible to latent cannot explain the higher integrated MSE, since sensible and latent heat contribute equally to MSE. A simple analysis of the surface energy budget revealed that the net shortwave radiation (downward) was nearly the same between WET and DRY, but the net longwave radiation (upward) in WET was about 100 W/m^2 less than DRY, due to the colder surface temperature. Also, the downward ground flux was about 100 W/m^2 larger in DRY than in WET, due to a higher surface skin temperature in DRY. As a result, the net LH+SH in WET is about 200 W/m^2 higher than in DRY. Assuming this additional flux sustains for 6 hours in a 1000-m PBL, this roughly gives an increase of MSE by about 4 K (MSE has a temperature unit in this paper). Note that near-surface MSE in WET is more than 20 K larger than DRY (Fig. 4), much larger than 4 K. Therefore, the changed radiation and ground heat conductance in WET creates a secondary yet significant apparent ‘source’ of MSE (more specifically, it is a reduction in heat losses to radiation and conduction in WET compared to DRY). Also note that the radiation effect here is different from that in Schar et al. (1999), where they referred to the more trapped longwave radiation by convective clouds in WET than in DRY at later stages.

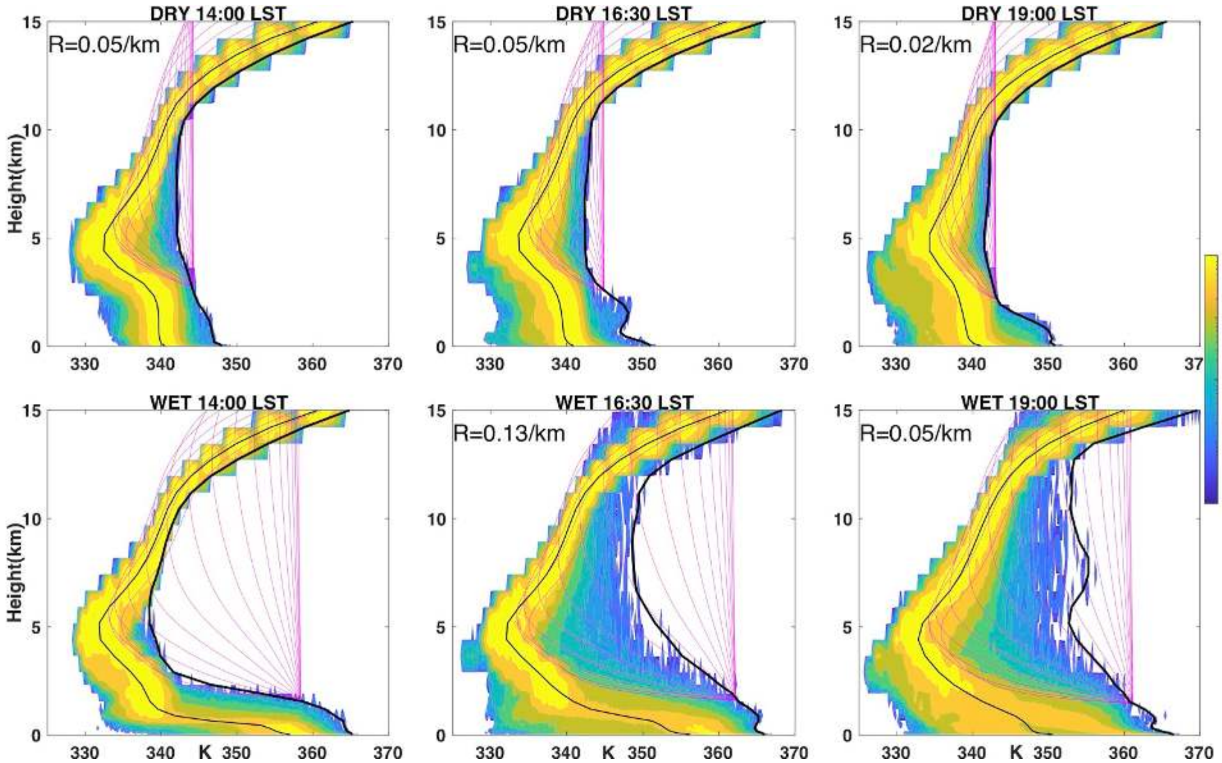

Figure 4. The time evolution of the probability distribution function (PDF, shading) of moist static energy (MSE, K) at each level for DRY (upper panels) and WET (lower panels). Thin and bolded black lines represent the domain mean and maximum MSE, respectively. The group of magenta lines in each panel represents the entraining plume model, where each line indicates the vertical MSE profile of a parcel decided only by a certain entrainment rate. The starting point of the parcel is at z = LCL and at the value of maximum MSE. Also shown in each panel is the entrainment rate fitted by the least squares of the maximum MSE profile between z = 3 and 10 km.

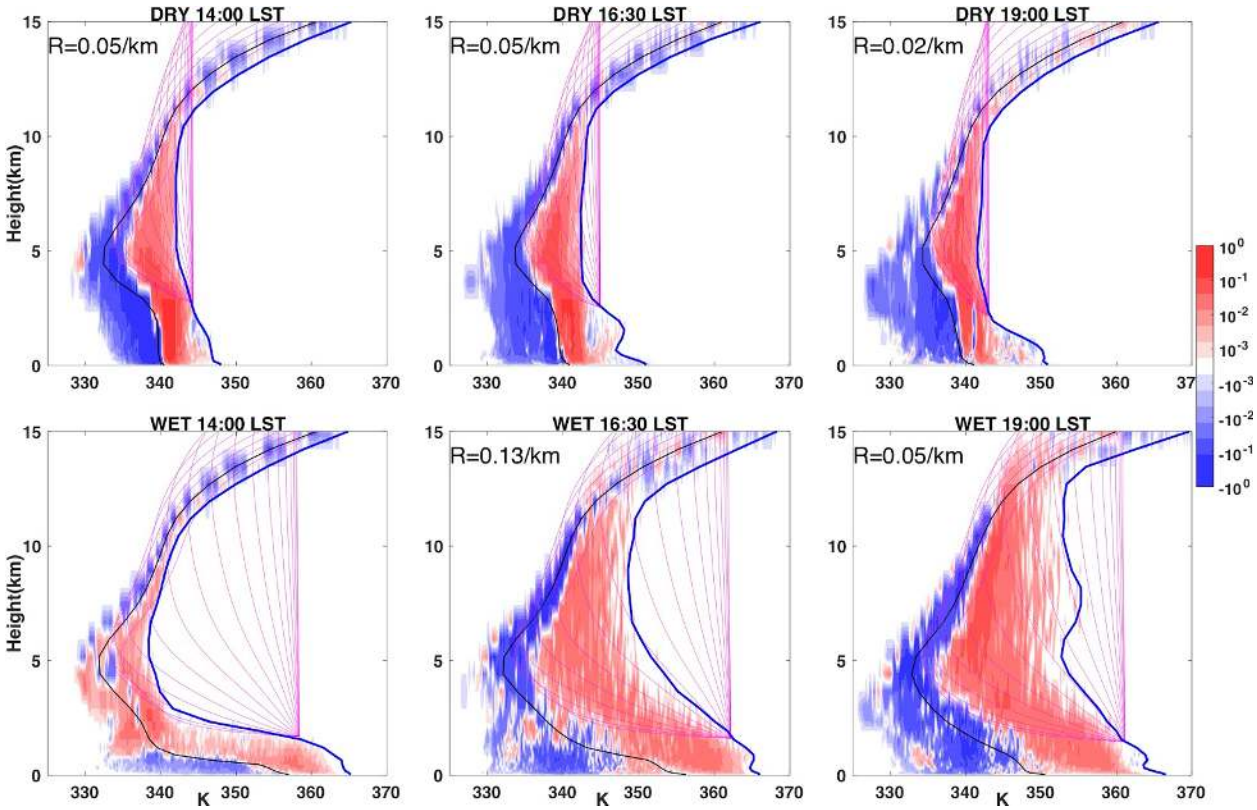

Figure 5. same as Figure4, except that the shading is the MSE-binned (0.2 K increment) vertical mass flux normalized across panels so that the range of the flux is between [-1 1]. The bolded blue line represents the maximum MSE.

4.1.2. Entraining plume model

A popular argument is that the cold pool can help organize convection by making clouds wider and thus reducing their entrainment rate (e.g., Kuang & Bretherton, 2005; Khairoutdinov & Randall, 2006; Schlemmer & Hohenegger, 2014). We want to see if this argument applies in our case, and if entrainment plays a role in the better organization of convection in WET compared to DRY. Here we followed the plume model method to estimate entrainment by Gentine et al. (2016), where, for a given entrainment rate, the vertical gradient of MSE in a parcel is only affected by the MSE difference between the parcel and the environment (similar to their Eq. 2) : $\frac{\partial MSE}{\partial z} = R(\overline{MSE} - MSE)$, where $\overline{MSE}$ is the horizontal mean MSE to approximate environmental MSE, R is the fractional entrainment rate, defined as the vertical gradient of the mass of cloud parcel divided by the mass of cloud parcel. As a result, the vertical profile of the parcel MSE can be uniquely defined (equation 3 of Gentine et al. 2016) for a constant entrainment rate: $MSE(z) = (MSE(LCL)e^{R\cdot LCL} + \int_{LCL}^{z} R \cdot \overline{MSE}(z')e^{R\cdot z'}dz')e^{-R\cdot z}$. By trying several entrainment rates one can estimate the rate as that which best fits a simulated profile. We defined the height of the starting point as the mean LCL where clouds are present. The starting MSE was the maximum MSE found at that LCL. The LCL was higher in DRY than in WET (as shown in Fig. 4 and Fig. 5), due to a warmer and drier PBL. The result of the plume model is shown in both Fig. 4 and Fig. 5 as a group of magenta lines in each subplot. Each line represents a vertical profile of MSE under one fixed entrainment rate. For example, the line where the MSE is constant with height means that the entrainment rate is 0.

The main distinction between DRY and WET is that parcels start with higher MSE in WET. In contrast, parcels in DRY start with an MSE value closer to the environment above the PBL, reflecting the deeper and more entraining PBL in DRY than in WET. Parcels are subjected to entrainment, reducing in-cloud MSE as they rise through the lower MSE air of the environment. In WET, the reduction of in-cloud MSE is steeper at earlier times in the development of the MCS, as inferred by the slope of the maximum MSE (thick blue lines in the lower panel of Fig. 5), which suggests a decrease in the entrainment rate over time. We quantitatively estimated the entrainment rate (R) by finding the value of R that predicts the best fit to the 3-point running mean maximum MSE profile (between z = 3-10 km), using the least squares method. R is systematically smaller in DRY than in WET at early times, as shown in Fig. 4 and Fig. 5. R further decreases slightly with time in DRY from 16:30 LST to 19:00 LST, although cold pools and convection are only active in the early stage in DRY (between 14:00 and 16:30 LST, see Fig. 3a, b). In contrast, R starts higher but decreases with time in WET as the convection in the MCS gets stronger (note that there is no value of R at 14:00 LST in WET because of the lack of convection at that time in the region of interest). Recalling that cold pools are more frequent (and colliding) early on in DRY and at later stages in the MCS evolution in WET (as in Fig. 3), we conclude that these entrainment estimates are consistent with the idea that cold pools help to reduce cloud entrainment by allowing wider, better organized clouds.

Therefore, the WET simulations support the idea that smaller entrainment rate with time indicates convective organization with larger clouds. However, the rising parcels in DRY have lower MSE and thus their profiles are less sensitive to entrainment due to similar in-cloud and environmental MSE values. This suggests that the environment selects for wider or larger cloud clusters (having lower entrainment rate) more so in WET than in DRY, such that entrainment (and hence cold pools) may have less impact on cloud size distributions in DRY. This idea is supported by cloud size distribution analyses at the end of Section 4.2.2 below.

4.2. The role of cold pools in MCSs

The cold pool is also hypothesized to have a significant impact on convective organization, because the cold pool-induced gust front, especially by colliding cold pools, can effectively trigger new convection (e.g., Rotunno et al., 1988; Schlemmer & Hohenegger, 2014; Feng et al., 2015; Haerter et al., 2019), so that the MSC can be maintained. It is straightforward to think that the stronger the cold pool evaporative cooling, the stronger the gust front, and the easier for new convection to be triggered. This idea is manifested in recent cold pool parameterizations (e.g., Rio et al., 2009; Grandpeix & Lafore, 2010; Del Genio et al., 2015), in which the gust front lifting ability is directly related to temperature deficits in cold pools. However, it needs to be kept in mind that if the cold pool is too strong, newly triggered convective cells will be too vertically slantwise or quickly detached from the surface source so that convection will be suppressed (Rotunno et al. 1988). These two potentially offsetting effects of cold pools on convection are key guidance for what is to be shown below.

As noted earlier, visual inspection of Fig. 3 shows more numerous cold pools in DRY at the early stage (Fig. 3a) despite better organization and stronger convection in WET at the mature stage (Fig. 3c). This indicates that the cold pool alone (without the environmental condition) does not determine the fate of the MCS. To see what happens after convective initiation, when the cold pool ceases to benefit convection, we examined both downdrafts and updrafts, as well as their relationships. We might expect that stronger low-level downdrafts would be coupled with stronger updrafts, in WET. To test this, we show the time evolution of the frequency distribution of vertical velocity (W, m/s) in the boundary layer for WET and DRY. The height of 250 m (upper panels of Fig. 6) was chosen to have clear signals of both cold pool downdrafts and gust front updrafts, and samples were chosen where it was cloudy. Early on, at 14:00 LST, DRY (blue line in Fig. 6a) has a much broader distribution of low-level W than WET (red line in Fig. 6a), simply because convection was triggered earlier in DRY. By 16:30 LST (Fig. 6b), convection in WET had caught up with DRY in terms of updraft and downdraft strength, per the wider distribution of W. However, considering all times together, peak low-level downdraft and updraft strengths in WET were very similar to those in DRY (compare the left-hand tails of the distributions of WET in Fig. 6b with those of DRY in Fig. 6a), suggesting that cold pool gust fronts were not a driving factor in explaining the stronger and better-organized MCS in WET. A look at mid-level updrafts gives yet another indication that gust fronts alone do not explain the stronger convection in WET, since updrafts at 6 km are much stronger in WET and the W distribution shows an asymmetric response at 6 km compared to that at lower levels. These results suggest that surface energy partitioning, specifically its effect on PBL state (vertical MSE profile) and CAPE, rather than cold pools, is responsible for the convective development in WET at later stages. The persistence of relatively strong low-level downdrafts at 19:00 LST in WET might in turn help sustain convection in WET, but appears secondary to the favorable low-level thermodynamic environment created by the WET surface.

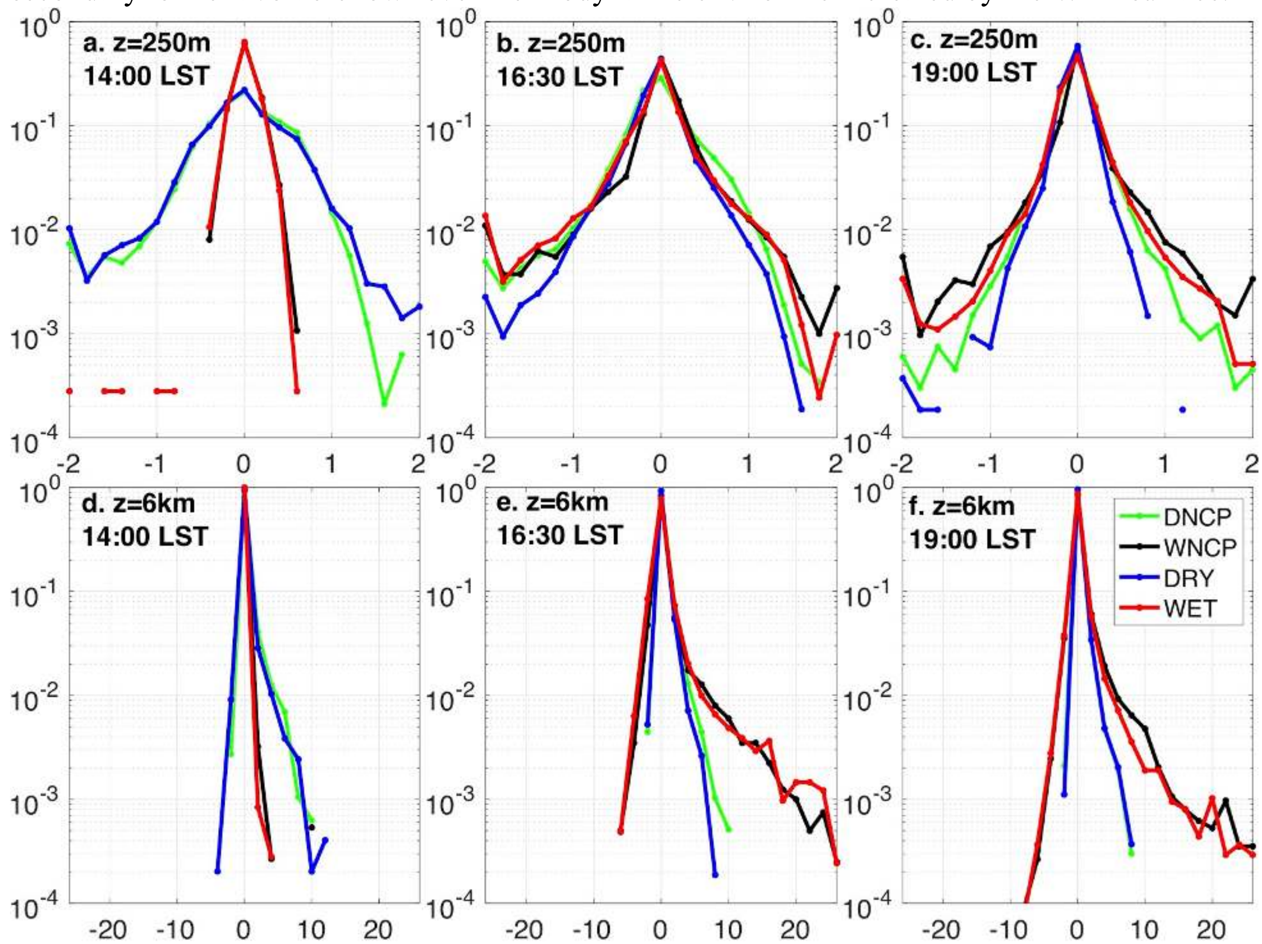

Figure 6. a-c. The relative frequency distribution of vertical velocity (m/s) at z = 250 m at 14:00, 16:30, and 19:00 LST for DRY (blue), WET (red), DNCP (green), and WNCP (black) simulations. b. Same as a, but for vertical

velocity (m/s) at z = 6 km. Logarithmic Y-axis is used for better visualization. 0 counts are not plotted due to the log scale.

4.2.1 "No-cold pool" experiments: Experimental setup

To better clarify the role of cold pools in convective organization, we have performed "no-cold pool" experiments by adjusting the Thompson microphysics. The most common way to remove cold pools in model experiments is to turn off the evaporation of rain (such as Khairoutdinov & Randall, 2006; Jeevanjee & Romps, 2013; Grant et al., 2018). That method should remove the cold air, but downdrafts below the convective updrafts could still exist because the downward dynamic pressure gradient force as well as hydrometeor loading effect is not removed. We have removed the hydrometeor loading effect (together with turning off evaporation in microphysics) in the vertical velocity equation, but found that the effect is minor when compared to evaporation. Note that, due to the dynamic pressure gradient force, convective downdrafts cannot be completely removed. Also, it is noteworthy that Rotunno and Klemp (1985) removed gust fronts by preventing rain production in the idealized simulations. We have done similar modifications, and found that their method is not feasible in realistic simulations with interactive radiation because the cloud-radiation interaction creates a large area of very cold air (not shown).

Given the above discussion, we show the "no-cold pool" simulations where only evaporation is turned off, so that other aspects of MCSs are as unaltered as possible. In order to keep the microphysics near the updraft region as unchanged as possible, we only turn off evaporation within the lowest 2 km, which is enough to "kill" most of the cold air in the cold pool region. Turning off the evaporation for the whole atmosphere was also tested, and we found similar results.

4.2.2 "No-cold pool" experiments: Comparison to "cold-pool" simulations

We ran "no-cold pool" experiments for both DRY and WET, hereafter named DNCP and WNCP respectively. We collectively refer to the cold-pool and no cold-pool experiments as CP and NCP. Even without rain-cooled air in the NCP simulations, gust fronts still exist (Fig. 7), but are not as numerous as in the CP simulations (Fig. 3). The gust front horizontal propagation is faster in CP than in NCP, which sweeps out a larger cold pool area and creates a larger area surrounded by gust fronts (Fig. 3 vs. Fig. 7). Greater horizontal spread indicates a greater chance for gust fronts to interact with the environmental air, and collide with each other. This is clear in the middle stage of DRY (Fig. 3b vs. Fig. 7b) and WET (Fig. 3e vs. Fig. 7e; Fig. 3f and Fig. 7f), where the total area of cold pools (surrounded by gust fronts) is larger in CP than NCP. We thus confirm that one important aspect of the cold pool is to provide more gust fronts for convective triggering and organization.

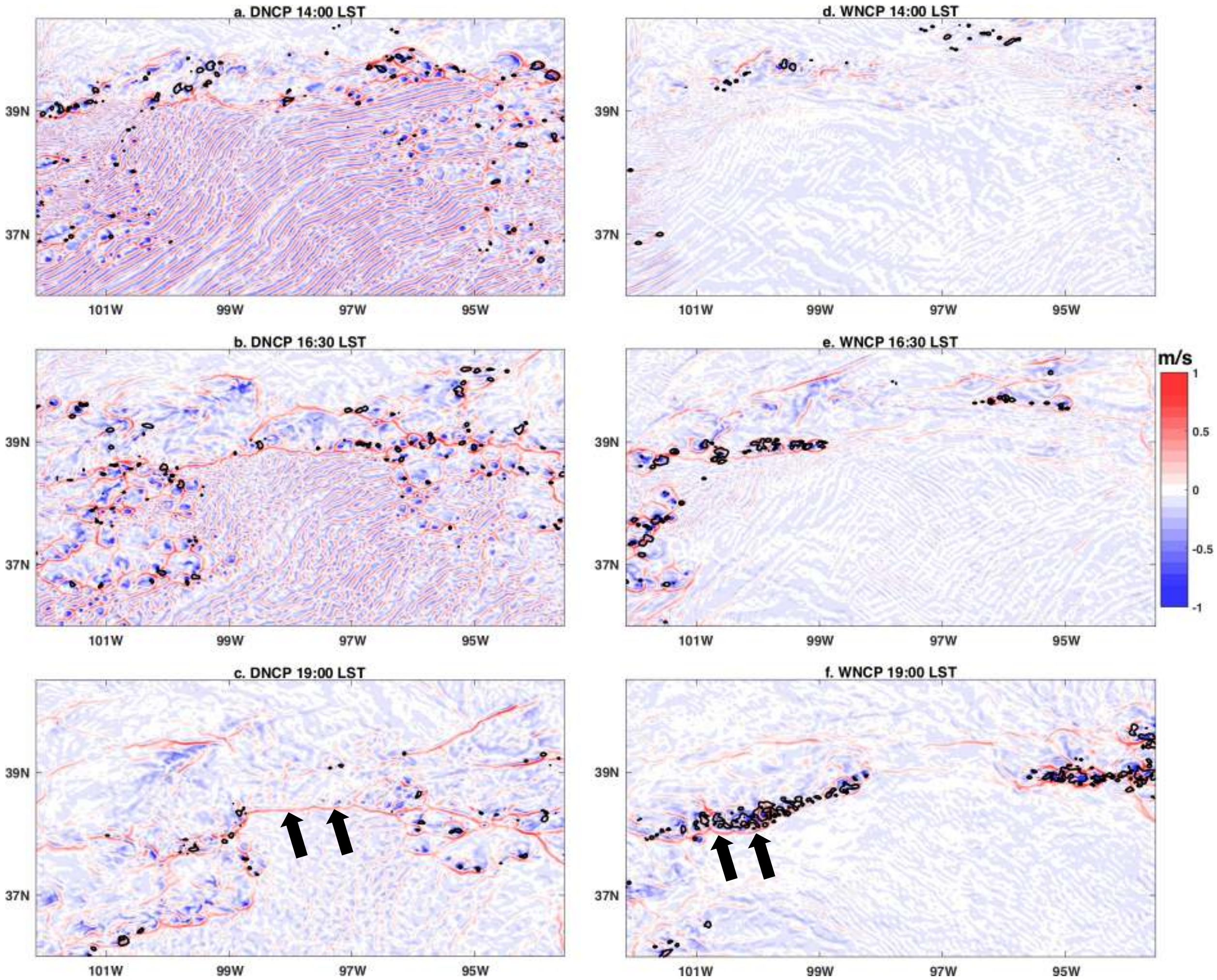

Figure 7. Same as Fig. 3, except for DNCP and WNCP simulations.

To check whether cold pools promote wider (less entraining) cloud clusters we compared convective cell sizes (Fig. 8) between CP and NCP experiments. Deep convective cells were defined where vertical velocity was larger than 0.7 m/s at z = 6 km. Data were separated into small cells (radius ≤ 6 km, Fig. 8a) and large cells (radius > 6 km, Fig. 8b). Dry-soil experiments had more small cells than wet-soil experiments (Fig. 8a), while the wet soil experiments had relatively more large cells (Fig. 8b). Furthermore, there were more small cells in WET than in WNCP, at all times (Fig. 8a), consistent with the hypothesis that vigorous cold pool gust fronts and their collisions promote triggering of new cells. The sensitivity in the DRY/DNCP experiments was limited to the early hours (14:00-16:30 LST) when convection is more active in those simulations.

Counterintuitively, however, the NCP simulations had comparable or even more large cells than CP (Fig. 8b). There were considerably more large cells in DNCP than in DRY, and WNCP had the greatest number (number = 20) of large cells (between 14:00-19:00 LST). Returning to the vertical velocity distribution (Fig. 6; black lines for WNCP, green lines for DNCP) we also see stronger low-level (250 m; top panels of Fig. 6) downdrafts and updrafts in NCP than in CP at 19:00 LST. The mid-levels (6km; bottom panels of Fig. 6) also show more moderately-strong updraft (around 10 m/s) in WNCP than WET, at 16:30 and 19:00 LST, indicating stronger convection in NCP simulations. Again, this is a bit counter-intuitive, because stronger cold pools in WET should have resulted in stronger and better organized convection, with larger cell sizes, unless something was working to offset or compete with that effect. Next, we explore that offsetting effect, in the region where good convective organization was found (the west part of Fig. 3f and Fig. 7f).

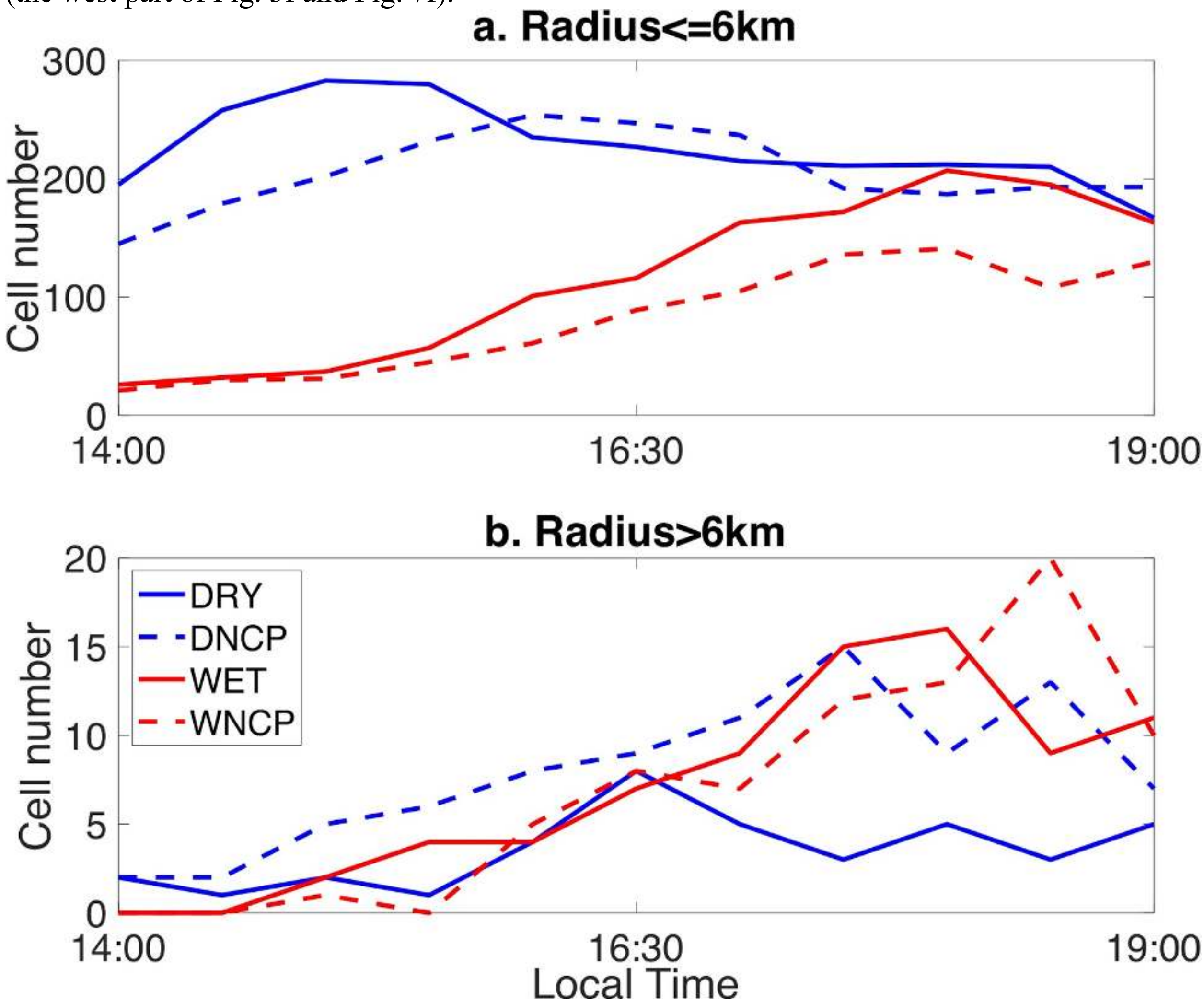

Figure 8. a. Time series of the number for small convective cells (radius ≤ 6 km) in each simulation. b. Same as a, except for large cells (radius > 6 km).

4.2.3 The offsetting effect of cold pools

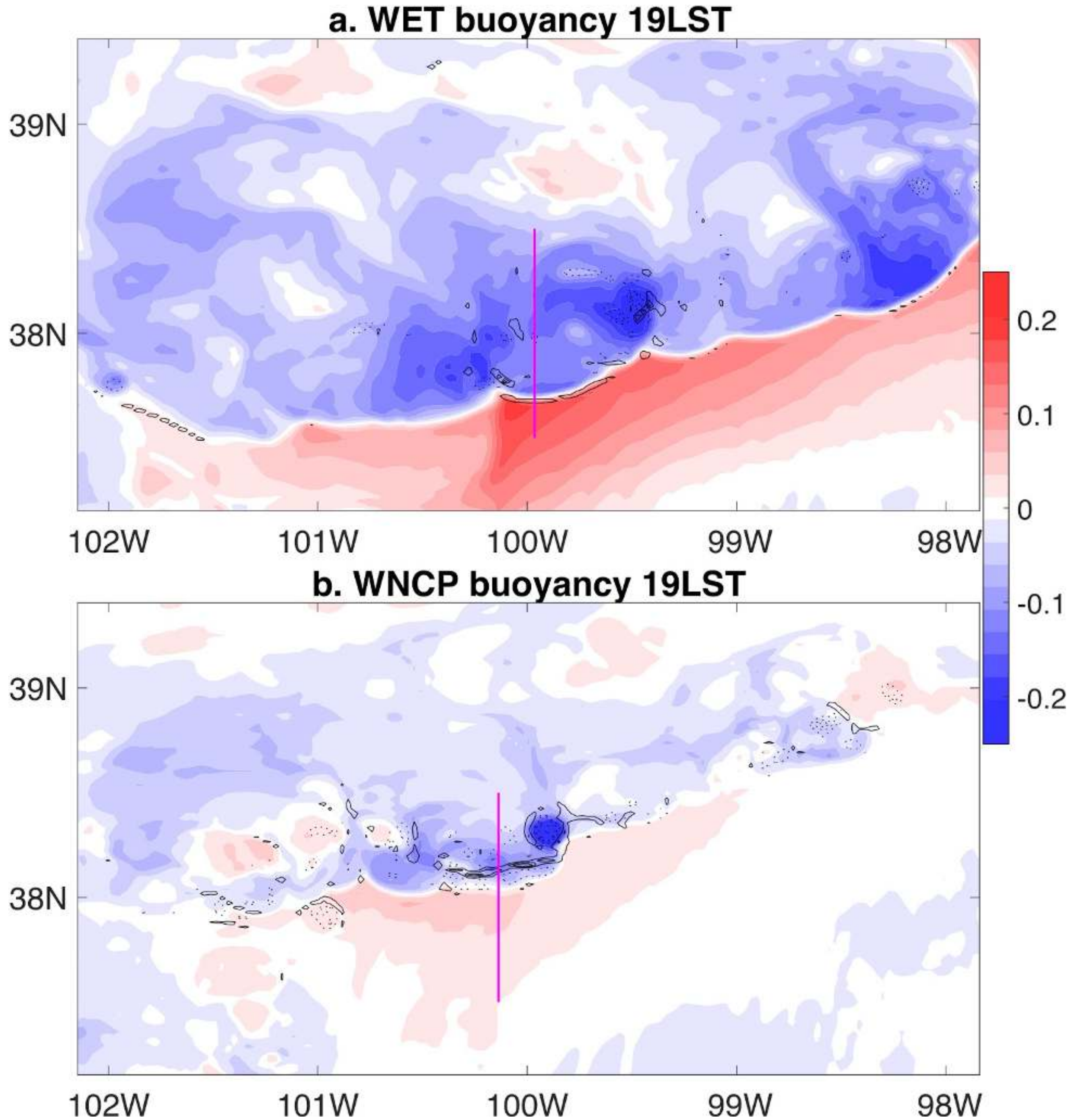

Figure 9. a. Buoyancy (shading, m s^{-2}, see definition in text) and divergence (s^{-1}, dashed contours are 0.003, 0.006, and 0.009; solid contours indicate convergence of -0.009, -0.006, and -0.003) in WET at t = 19 LST; Magenta line indicates the vertical cross section that is to be shown in Figure 10. b. same as a, except for WNCP.

Conceptually, we consider the horizontal propagation of the gust front separately from the strength of the horizontal wind itself. Namely, we note that the dense air in cold pools spreads laterally and pushes the gust front farther away from convective cores, while the downdraft brings higher momentum air downward and thus contributes to the strength of the horizontal wind gust. Hydrometeor loading and dynamic pressure gradient forces contribute to downdrafts, forming gust fronts even without evaporative cooling of rain, but they do not necessarily help to propagate the gust fronts horizontally beyond what is required by continuity of mass. Thus, the horizontal propagation of gust fronts could be greater in CP compared to NCP due to the greater density of the evaporatively-cooled air in CP, which may explain the weaker convective updrafts/downdrafts and smaller cell sizes in CP. For example, in Rotunno et al. (1988), if the cold pool is too strong, newly triggered convection becomes slanted toward cold pool side and detached from the surface gust front.

We first verified that CP simulations indeed have denser cold pool air (lower or more negative cold pool buoyancy) than NCP, which may not be obvious due to less hydrometeor loading in CP simulations (from the removal of rain drops by evaporation). We used buoyancy ($m\ s^{-2}$, shading in Fig. 9) to compare the low-level thermodynamics between WET and WNCP. Similar to previous studies (such as Tompkins 2001 and Feng et al. 2015), buoyancy is defined here as $B = g(\theta_\rho - \overline{\theta_\rho})/\overline{\theta_\rho}$, where the overbar is a running mean value from a 200 km by 200 km box centered on a given point, in order to get a local (relative) buoyancy given the large area we are simulating (following Feng et al., 2015). θ_ρ is the density potential temperature (K) defined as $\theta_\rho = \theta(1 + 0.608q_v - q_{cloud} - q_{rain})$, where θ is potential temperature, and q_v, q_{cloud}, and q_{rain} represents the mass mixing ratios of water vapor, cloud droplets, and rain water, respectively. Note that θ_ρ already includes the effect of hydrometeor loading. In simulations where evaporation is not allowed, $(1 + 0.608q_v - q_{cloud} - q_{rain})$ in the cold pool region will clearly decrease due to the decrease of water vapor and increase of hydrometeor loading, given the same total water content. But it turns out that the enhanced θ (because no evaporative cooling below z = 2 km) more than enough offsets the hydrometeor loading effect, making θ_ρ in the "cold pool" region warmer, and creating a much weaker *B* in the "cold pool" region in WNCP (Fig. 9b) than that in WET (Fig. 9a); note that we do find a small area of strong negative buoyancy in WNCP, which is a result of very dense precipitation there.

Based on the above thermodynamic analysis, the much stronger negative *B* (denser air cold pools air) in WET is indeed consistent with the faster horizontal gust front propagation in WET compared to WNCP (Fig. 9a vs. Fig. 9b).

To see if the gust front propagation speed can explain the stronger, larger convective cells in WNCP, we show a cross section of the secondary circulation (the meridional and vertical wind) in Fig. 10. The vertical cross section was taken along the 99.9° W longitude line in WET (100.1° W in WNCP), which is aligned nearly perpendicular to the gust front (indicated by the magenta lines in Fig. 9). When cold pool downdrafts reach the surface, the strong horizontal wind (yellow shading in Fig. 10) spreads over a larger horizontal distance (about 70 km) in WET compared to WNCP (35 km). Since the cold pool air is much colder and denser than the surrounding environment in WET than in WNCP, the cold air tends to intrude below the warm air, instead of directly colliding with the warm air. The propagation of the gust front in WET is thus 'too fast' such that newly triggered convective cells are detached horizontally from the old convective cells that create the cold pool (red contours in Fig. 10a). The lifting of environmental air behind gust fronts in WET follows a very slantwise trajectory upward (white line in Fig. 10a). In contrast, the downdraft air and the environmental air in WNCP are forced almost directly upward once they interact, because there is almost no density difference (Fig. 9b) between them.

We conclude that the more upright interface slope between the downdraft air and the environment in WNCP (white line in Fig. 10b) explains why it has even more robust convection than WET. The smaller distance between newly triggered and old convective cells in WNCP (red contours in Fig. 10b) also favors stronger convection and possible merger of convection.

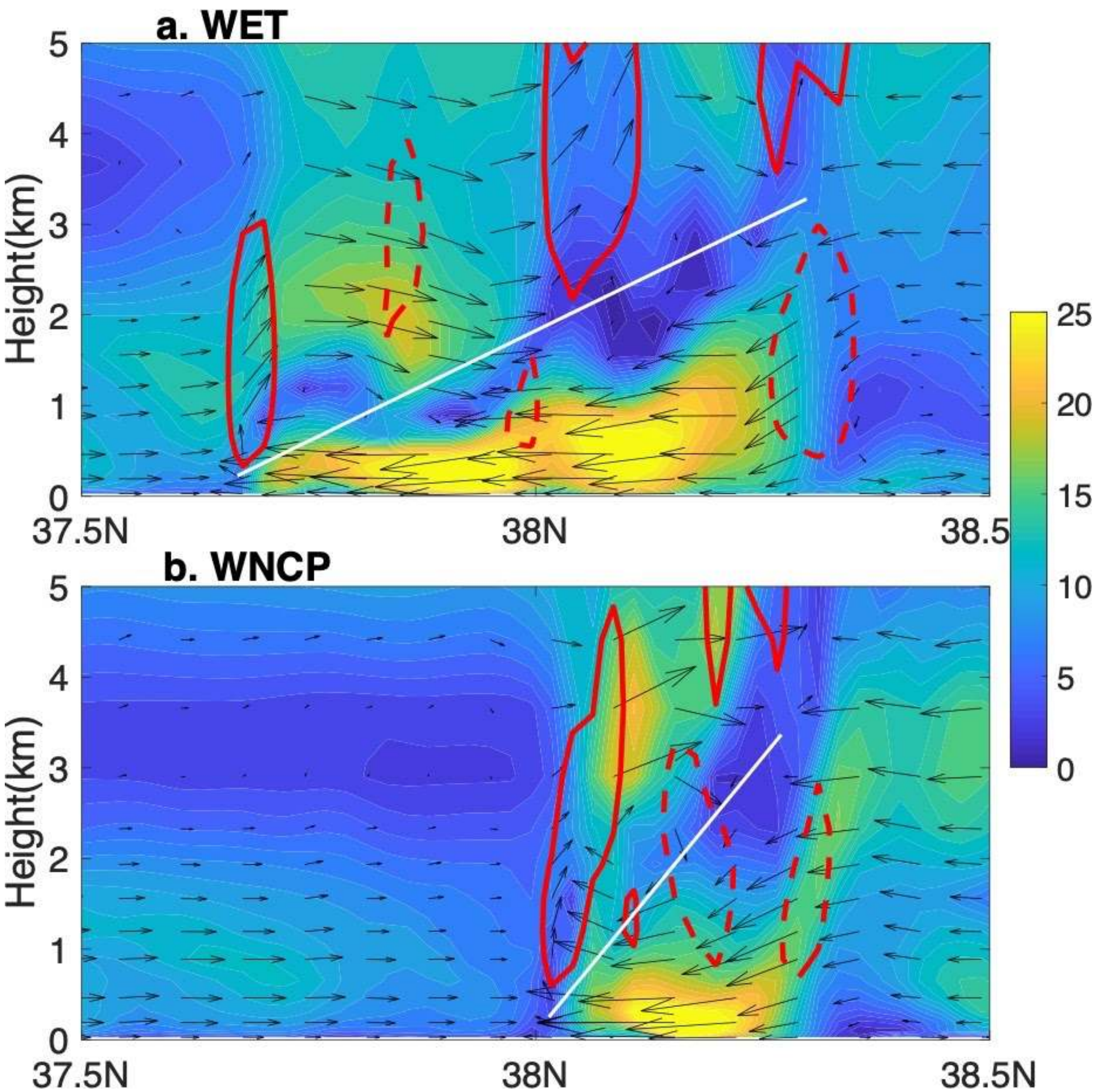

Figure 10. a. Vertical cross section of horizontal wind speed (shading) and secondary circulation at 19:00 LST (vectors indicate meridional wind V and vertical velocity W; note that W is multiplied by 2.5 for visualization). Red solid line indicates W = 2 m/s; red dashed line indicates W = -2 m/s. b. same as *a*, except for WNCP.

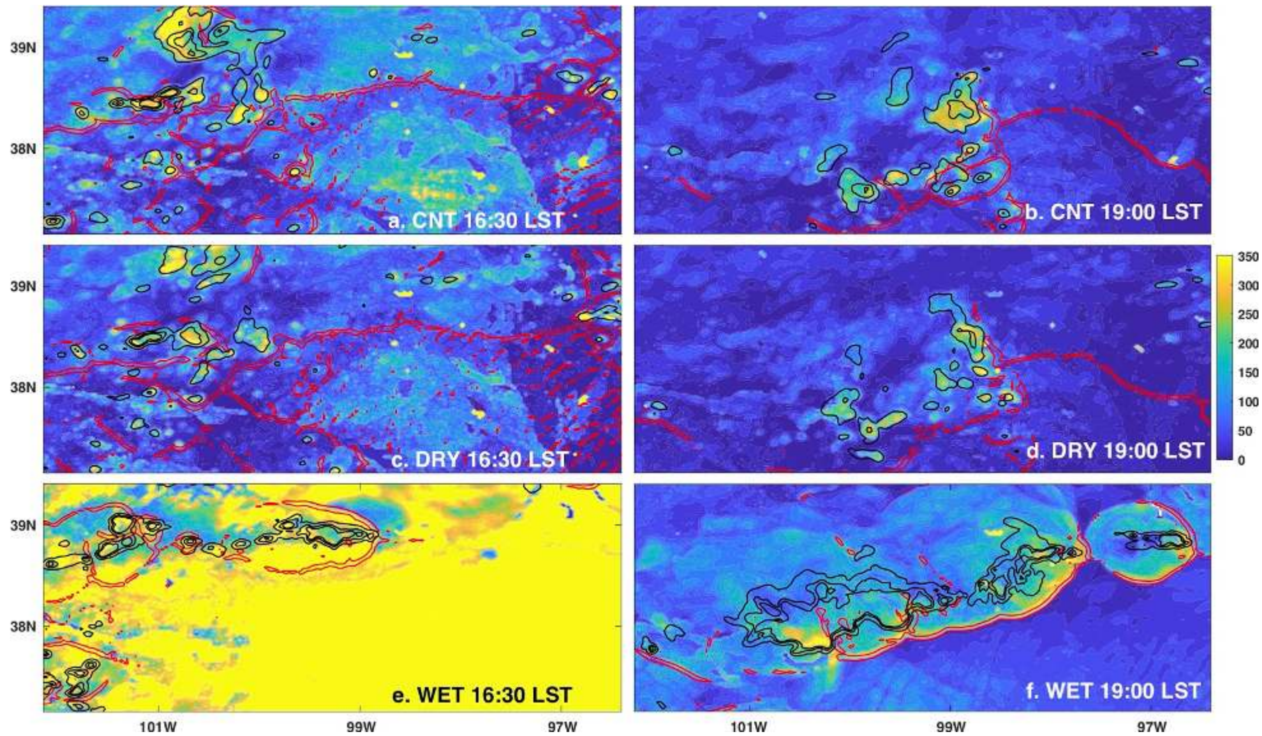

Figure 11. Surface latent heat flux distribution (shaded) for CTL (a and b), DRY (c and d), and WET (e and f), at 16:30 and 19:00 LST. Red contours represent vertical velocity of 0.5 m/s at z = 200 m to indicate gust fronts; Black contours represent rain rates of 1, 5, and 10 mm/hour.

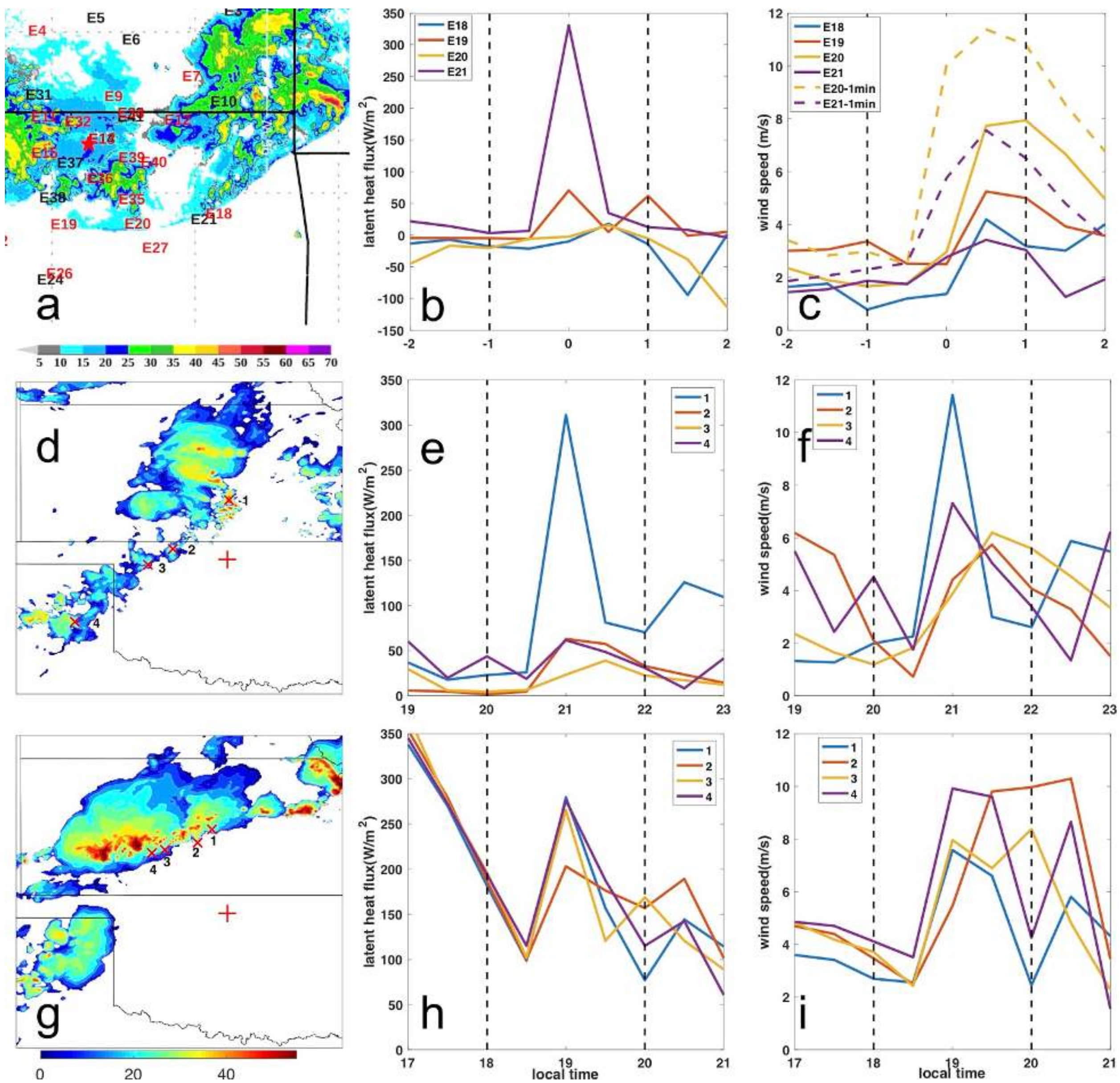

Figure 12. a. Radar reflectivity (dBZ) from NEXRAD at 21 LST on August 10th, 2006. Red star indicates the SGP main site. Red site labels indicate EBBR sites, while black labels indicate ECOR sites. b and c are the time series of latent heat flux and surface wind speed for site E18, 19,20, and 21. Time 0 indicates the passage of the gust front. The dashed lines in c are the maximum wind speed in every 30-minute interval using the MET 1-min data, for E20 and E21. The middle panels (d-f) are the same as the upper panels, except for model data in the control run (CTL) around 21 LST. Red crosses indicate the model grid points chosen for comparison to observations. Wind speed is calculated by 10-meter instantaneous U and V from the model output. The lower panels (g-i) are the same as the middle panels, except for model data in WET around 19 LST.

4.3 Surface wind and latent heat flux

Finally, we turn to the third mechanism of surface influence on convective organization, involving surface flux interactions. If an MCS is to persist beyond sunset, it must resist the detrimental effect of reduced (solar) energy available for surface sensible (SH) and latent heat flux (LH). As such, a positive feedback between surface LH and convection could be important for convective organization after sunset (note that we did not consider SH here, because SH was much weaker than LH by late afternoon). Specifically, we ask: can cold pools and gust fronts enhance the surface LH even after sunset when energy is limited?

4.3.1 Latent heat flux in the model

As expected, all simulations had weaker surface LH outside of the MCS region after sunset at 19:00 LST (right panels in Fig. 11) compared to 16:30 LST (left panels in Fig. 11). However, LH within the gust fronts was still strong at 19:00 LST, particularly in WET (Fig. 11f). Thus, cold pools and the associated gust fronts are able to enhance or maintain strong LH after sunset when the atmospheric energy supply for evaporation is already limited. The LH at 19:00 LST within the MCSs in CTL and DRY was also higher (comparable with that at earlier daytimes), but only in areas near precipitation. We conclude that WET is most consistent with a positive feedback on MCS growth, which would require the convection-enhanced surface LH to be spatially correlated with new convection: most of the strong LH was located near leading gust fronts in WET (red contours in Fig 11f), so that the LH could effectively feed back onto newly triggered convective cells, making the MCS stronger and longer-lasting. Note that the high LH along the gust front edge not only occur at 19:00 LST: it persists with time as gust fronts propagate (at least in our 30-minute model output).

4.3.2 ARM surface observations

The surface observation network provides an opportunity to evaluate the model wind gusts and to see whether the passage of the gust front is correlated with an enhancement of LH. In fact, a gust front was captured in observations across the SGP site around 21:00 LST in the 2006-08-10 MCS case. A northeast-southwest gust front to the southeast of the SGP site (shown as the red star in Fig. 12a) is clear around 21:00 LST in the radar maximum reflectivity from the NEXRAD system (Fig. 12a). Four observational sites recorded this event, including three energy balance Bowen ratio systems (sites E18, E19, and E20; all grassland sites) and one eddy-covariance instrument (E21; an oak forest). Using the 4 sites, 30-min mean LH and near-surface wind speed are plotted in Fig. 12b and 12c. We defined hour 0 as the time when the gust front passed each site (around 19:00 LST at most sites, and 20:00 LST at site E19). Model surface wind speed was taken from the instantaneous 10-meter wind output. We used observational data at 1-minute temporal resolution where available (sites E20 and E21), and chose the maximum 1-minute wind within each 30-minute range from the ARM Surface Meteorology Systems (MET) dataset, to be consistent with instantaneous model output at the chosen grid cells near the gust front.

All sites showed an increase in LH as the gust front passed (Fig. 12b), although the variation of the magnitude was large. E21 saw the largest increase (spike) in LH despite having the smallest increase in wind speed, which may reflect higher canopy water vapor content at E21 relative to other sites (E21 is the only forested site here), as discussed further below. To show the model surface wind and LH at scales similar to the observation, we chose three grid points (red crosses in Fig. 12d) in the control run (CTL) along the gust front (points 2-4 in Fig. 12d); and (for reasons given below) one additional point near convective cells with precipitation (point 1 in Fig. 12d). Likewise, the lower panels of Fig. 12 show the results of WET at selected sites along the gust front.

The spike in LH was similar in magnitude between observations and CTL (Fig. 12b, e) at the time of gust front passage. However, in CTL the LH spike was confined to areas with precipitation behind the gust front (model point 1), whereas it occurred along the gust front edge in observations and in WET (lower panels of Fig. 12; and Fig. 11f). Thus, it is possible that the model (CTL) is not able to represent the effect of land surface heterogeneity on surface heat fluxes, while erroneously emphasizing the effect of precipitation 'recycling'. In particular, forest canopy storage of water vapor is not represented in CLM, which may have limited the model's LH along the gust front edge in CTL. However, whether this is the true physical explanation for the observation at the E21 forest needs further investigation beyond this study.

Our results suggest that feedback of convection-induced wind gusts on surface LH could be an important factor helping MCSs to persist after sunset. Both model and observation confirm an enhancement of LH during passage of a gust front. Furthermore, the strong LH near gust fronts (strong wind) instead of within cold pools (precipitation) is effective in supporting the newly triggered convection, as seen in the WET simulation. This result provides a realistic case to support earlier conclusions based on idealized model experiments, on the importance of interactive surface heat fluxes (Gentine et al., 2016; Grant & Van den Heever, 2018).

5. Discussion and Conclusion

In summary, three main results were obtained on the roles of surface energy partitioning in convective organization (MCSs) near the US SGP site: (1) Wetter soil (higher surface latent heat flux relative to sensible) leads to a stronger MCS at later stages than drier soil in most of our simulated cases, regardless of the earlier convective initiation in many of the drier soil experiments; (2) although the cold pool helps trigger new convection, it can also offset convection by making updrafts slantwise; and (3) cold pools allow MCSs to maintain large latent heat flux (along leading gust-fronts) into nighttime.

Three possible mechanisms by which the cold pool could serve as an agent in the land-convection coupling were explored: entrainment, ascent along gust fronts (particularly in high-CAPE environments), and surface flux interactions. Entrainment rate was in general smaller in DRY than WET, consistent with more numerous small cold pools (and their collisions) creating larger clouds in the early afternoon in DRY. However, the build-up of MSE in the shallower boundary layer in WET (and hence larger CAPE) becomes more important later in the MCS development, ultimately favoring better organized MCSs in WET than DRY. Thus, while past (smaller-domain studies) suggested that the cold pool collision is a main mechanism to promote convection, our larger-domain study indicates that the large-scale modification of CAPE by surface fluxes can ultimately determine the degree of convective organization and intensity at later mature stages of the MCS. In addition, while the cold-pool-induced gust fronts provide the uplift to trigger new convection, the dynamic (pressure perturbation) contribution to gust front uplift makes this mechanism relatively insensitive to cold-pool density (negative buoyancy), as discussed in further detail below. Nevertheless, the land-atmosphere difference created by cold pool properties (dry, cold air, and strong gust-front wind) could help to increase or maintain surface heat fluxes, potentially promoting convective organization.

Given what has been learnt about cold pools in this study, the cold pool parameterizations can be potentially improved. In previous cold pool parameterizations, the gust front lifting ability is proportional to the negative-buoyancy-induced horizontal propagation speed (or cold pool intensity), which is associated with the evaporative cooling of hydrometeors (e.g. Rio et al., 2009; Grandpeix & Lafore, 2010; Del Genio et al., 2015). However, strong cold pools might not be as efficient to lift environmental air as calculated by these cold pool parameterizations, because a slantwise interface slope between the density current and environment will substantially weaken the gust front uplift, as seen in our CP and NCP comparisons. The interface slope can be easily incorporated into the cold pool parameterizations by introducing a parameter associated with the density difference between cold pool and environmental air. The slope may explain the need for tunable parameters in cold pool parameterizations, which may need to be modified to accommodate different microphysics schemes. For example, in Rio et al. (2009), the lifting energy of gust fronts is only half of the wake potential energy (see their auxiliary material), which might be a compromise of the slope of the updraft.

The enhancement of LH during the passage of a weak gust front at night in both the model and observation suggests a positive feedback between surface fluxes and convective organization. It may be noted that we focused only on locally forced MCSs in this study: many simulated cases are less well-organized MCSs with more scattered convection, instead of 'text-book' MCSs whose convection is stronger and more clustered. To what extent this local forcing (surface energy partitioning) is important compared to other factors (such as low-level jet and vertical wind shear) needs further investigation.

By resolving convection, the current simulations not only confirm previous findings (e.g., Schar et al., 1999; Findell & Eltahir 2003b) that more precipitation occurs over wetter soil, but also emphasize that the resolved convective organization and cold-pool gust front are responsible processes. How to accurately represent those processes in convection-parameterized climate models is a persistent problem. In addition to the potential advantage by incorporating the adverse (depending on environmental wind shear) effects of strong cold pools into cold pool parameterizations, this study also suggests that the coupling between cold pools and the interactive land surface could help convection persist into the night, and is worth further exploring in terms of parameterization. Lastly, the role of cold pools on convection differs at different stages, casting doubts on cold pool parameterizations that only focus on one aspect. Thus, stage-dependent processes might be needed to represent cold-pool effects on convective organization in Earth system models.

Acknowledgments

The model output is accessible from https://portal.nersc.gov/project/m2574/. This research is supported by the U.S. Department of Energy, Atmospheric System Research, and Atmospheric Radiation Measurement Programs, under contract DE-AC02-05CH11231. Observational data for the SGP sites were obtained from the ARM archive (http://www.archive.arm.gov/discovery/), from the following datastreams: ECOR (http://dx.doi.org/10.5439/1025039): sgp30ecorE21.b1, EBBR (http://dx.doi.org/10.5439/1023895): sgp30ebbrE18.b1, sgp30ebbrE19.b1, and sgp30ebbrE20.b1, MET (http://dx.doi.org/10.5439/1025220): sgpmetE20.b1 and sgpmetE21.b1. Numerical simulations are performed partly at the National Energy Research Scientific Computing Center (NERSC), supported by the Office of Science of the U.S. Department of Energy under contract DE-AC02-05CH11231, and partly at the Extreme Science and Engineering Discovery Environment (XSEDE), which is supported by National Science Foundation grant number ACI-1548562, with the allocation ID: ATM190016. The first author also acknowledges the suggestions from Dr. Jimy Dudhia and Dr. Joseph Klemp at NCAR, for helping remove the hydrometeor effect in the WRF code.

References:

Chen, S.-H. and W.-Y. Sun (2002). A one-dimensional time dependent cloud model. *J. Meteor. Soc. Japan.*, *80*(1), 99–118.

Dai, A., F. Giorgi, and K. E. Trenberth (1999). Observed and model simulated diurnal cycles of precipitation over the United States, *J. Geophys. Res.*, *104*, 6377–6402, doi:10.1029/98JD02720.

Del Genio, A.D., J. Wu, A.B. Wolf, Y. Chen, M. Yao, and D. Kim (2015). Constraints on Cumulus Parameterization from Simulations of Observed MJO Events. *J. Climate, 28*, 6419–6442.

Feng, Z., L. R. Leung, S. Hagos, R. A. Houze, C. D. Burleyson, and K. Balaguru (2016). More frequent intense and long-lived storms dominate the springtime trend in central US rainfall. *Nat. Commun., 7*, 13429.

Feng, Z., S. Hagos, A. K. Rowe, C. D. Burleyson, M. N. Martini, and S. P. de Szoeke (2015), Mechanisms of convective cloud organization by cold pools over tropical warm ocean during the AMIE/DYNAMO field campaign, *J. Adv. Model. Earth Syst., 7*, 357–381.

Findell, K. L., and E A B Eltahir (2003). Atmospheric controls on soil moisture-boundary layer interactions. Part I: Framework development. *Journal of Hydrometeorology*, *4*(3), 552-569.

Findell, K. L., and E A B Eltahir (2003). Atmospheric controls on soil moisture-boundary layer interactions: Three-dimensional wind effects. *Journal of Geophysical Research*, *108*(D8), 8385.

Fritsch, J. M., R. J. Kane, and C. R. Chelius (1986). The contribution of mesoscale convective weather systems to the warm-season precipitation in the United States. *J. Climate Appl. Meteor., 25*, 1333–1345.

Froidevaux, P., L. Schlemmer, J. Schmidli, W. Langhans, and C. Schär (2014). Influence of the Background Wind on the Local Soil Moisture–Precipitation Feedback. *J. Atmos. Sci., 71*, 782–799.

Gantner, L., and N. Kalthoff (2010). Sensitivity of a modelled life cycle of a mesoscale convective system to soil conditions over West Africa. *Quart. J. Roy. Meteor. Soc., 136*, 471–482.

Gentine, P., A. Garelli, S.-B. Park, J. Nie, G. Torri, and Z. Kuang (2016). Role of surface heat fluxes underneath cold pools, *Geophys. Res. Lett., 43*, 874–883.

Gentine P, A. Holtslag, F D'Andrea , and M Ek (2013). Surface and Atmospheric Controls on the Onset of Moist Convection over Land. *Journal of Hydrometeorology.* 14:1443-1462.

Grandpeix, J. and J. Lafore (2010). A Density Current Parameterization Coupled with Emanuel's Convection Scheme. Part I: The Models. *J. Atmos. Sci., 67*, 881–897.

Grant, L. D., & van den Heever, S. C. (2018). Cold pool-land surface interactions in a dry continental environment. *Journal of Advances in Modeling Earth Systems, 10*, 1513–1526.

Grant, L.D., T.P. Lane, and S.C. van den Heever (2018). The Role of Cold Pools in Tropical Oceanic Convective Systems. *J. Atmos. Sci., 75*, 2615–2634.

Guillod, B., Orlowsky, B., Miralles, D. et al. (2015). Reconciling spatial and temporal soil moisture effects on afternoon rainfall. Nat Commun 6, 6443. https://doi.org/10.1038/ncomms7443.

Haerter, J. O., Böing, S. J., Henneberg, O., & Nissen, S. B. (2019). Circling in on convective organization. *Geophysical Research Letters, 46*, 7024–7034.

Houze, R. A., Jr. (1994). *Cloud Dynamics*. International Geophysics Series, Vol. 53, Academic Press, 573 pp.

Hohenegger, C., P. Brockhaus, C.S. Bretherton, and C. Schär (2009). The Soil Moisture–Precipitation Feedback in Simulations with Explicit and Parameterized Convection. *J. Climate, 22*, 5003–5020.

Iacono, M. J., J. S. Delamere, E. J. Mlawer, M. W. Shephard, S. A. Clough, and W. D. Collins (2008). Radiative forcing by long–lived greenhouse gases: Calculations with the AER radiative transfer models. *J. Geophys. Res.*, *113*, D13103.

Jeevanjee, N., and D. M. Romps (2013). Convective self-aggregation, cold pools, and domain size, *Geophys. Res. Lett., 40*, 994–998.

Jeevanjee, N. and D.M. Romps (2015). Effective Buoyancy, Inertial Pressure, and the Mechanical Generation of Boundary Layer Mass Flux by Cold Pools. *J. Atmos. Sci., 72*, 3199–3213.

Khairoutdinov, M. and D. Randall (2006). High-Resolution Simulation of Shallow-to-Deep Convection Transition over Land. *J. Atmos. Sci., 63*, 3421–3436.

Konings AG, GG Katul GG, and A. Porporato (2010). The rainfall-no rainfall transition in a coupled land-convective atmosphere system. *Geophys Res Letters,* 37:L14401.

Koster, R. D., Suarez, M. J., Higgins, R. W., & Van den Dool, H. M. (2003). Observational evidence that soil moisture variations affect precipitation. *Geophysical Research Letters, 30*(5), 1241.

Kuang, Z., and C. S. Bretherton (2005). A mass-flux scheme view of a high-resolution simulation of transition from shallow to deep cumulus convection. *J. Atmos. Sci., 63*, 1895–1909.

Lawrence, D. M., et al., 2011: Parameterization improvements and functional and structural advances in Version 4 of the Community Land Model. *J. Adv. Model. Earth Syst.*, **3**, M03001.

Lu, Y., and L. M. Kueppers (2012). Surface energy partitioning over four dominant vegetation types across the United States in a coupled regional climate model (Weather Research and Forecasting Model 3–Community Land Model 3.5). *J. Geophys. Res.*, *117*, D06111.

Markowski, P., and Y. Richardson (2011). *Mesoscale Meteorology in Midlatitudes*. Vol. 2. Wiley-Blackwell, 430 pp.

Minnis, P., Nguyen, L., & Palikonda, R. (2008). Near-real time cloud retrievals from operational and research meteorological satellites. *Remote Sensing of Environment*.

Nakanishi, M., and H. Niino (2009). Development of an improved turbulence closure model for the atmospheric boundary layer. *J. Meteor. Soc. Japan*, *87*, 895–912.

Pfeifroth, U., R. Hollmann, and B. Ahrens (2012), Cloud cover diurnal cycles in satellite data and regional climate model simulations, *Meteorol. Z*., 21(6), 551– 560.

Rio, C., F. Hourdin, J.-Y. Grandpeix, and J.-P. Lafore (2009). Shifting the diurnal cycle of parameterized deep convection over land, *Geophys. Res. Lett., 36*, L07809.

Qiu, S. and I.N. Williams (2020). Observational evidence of state-dependent positive and negative land surface feedback on afternoon deep convection over the Southern Great Plains. *Geophysical Research Letters*, 47, e2019GL086622.

Rotunno, R. and J. Klemp (1985) On the Rotation and Propagation of Simulated Supercell Thunderstorms. *J. Atmos. Sci., 42*, 271–292.

Rotunno, R., J.B. Klemp, and M.L. Weisman (1988). A Theory for Strong, Long-Lived Squall Lines. *J. Atmos. Sci., 45*, 463–485.

Schär, C., D. Lüthi, U. Beyerle, and E. Heise (1999). The Soil–Precipitation Feedback: A Process Study with a Regional Climate Model. *J. Climate, 12*, 722–741.

Schlemmer, L. and C. Hohenegger (2014). The Formation of Wider and Deeper Clouds as a Result of Cold-Pool Dynamics. *J. Atmos. Sci., 71*, 2842–2858.

Skamarock, W. C., and Coauthors (2008). A description of the Advanced Research WRF version 3. *NCAR Tech. Note* NCAR/TN-475+STR, 113 pp.

Squitieri, B. J., and W. A. Gallus, 2016: WRF Forecasts of Great Plains Nocturnal Low-Level Jet-Driven MCSs. Part I: Correlation between Low-Level Jet Forecast Accuracy and MCS Precipitation Forecast Skill. *Wea. Forecasting*, 31, 1301–1323.

Tang, S., Xie, S., Zhang, M., Tang, Q., Zhang, Y., Klein, S. A., et al. (2019). Differences in eddy-correlation and energy-balance surface turbulent heat flux measurements and their impacts on the large-scale forcing fields at the ARM SGP site. *Journal of Geophysical Research: Atmospheres*, 124, 3301–3318.

Taylor, C. M., R. A. M. De Jeu, F. Guichard, P. P. Harris, and W. A. Dorigo (2012). Afternoon rain more likely over drier soils, *Nature,* 489, 423–426

Thompson, G., P. R. Field, R. M. Rasmussen, W. D. Hall (2008). Explicit Forecasts of Winter Precipitation Using an Improved Bulk Microphysics Scheme. Part II: Implementation of a New Snow Parameterization. *Mon. Wea. Rev.*, *136*, 5095–5115

Tompkins, A.M. (2001). Organization of Tropical Convection in Low Vertical Wind Shears: The Role of Cold Pools. *J. Atmos. Sci., 58*, 1650–1672

Torri, G., Z. Kuang, and Y. Tian (2015). Mechanisms for convection triggering by cold pools, *Geophys. Res. Lett., 42*, 1943–1950, doi:10.1002/2015GL063227.

Williams, I. N. (2019). Evaluating soil moisture feedback on convective triggering: Roles of convective and land-model parameterizations. *Journal of Geophysical Research: Atmospheres, 124*, 317–332.

Williams, I.N., J. Lee, J. Tadic, Y. Zhang, and H. Chu (2020). Modeling spatial heterogeneity in surface turbulent heat flux in the US Southern Great Plains, *Journal of Geophysical Research: Atmospheres, 125*, e2019JD032255.

Yang, G. and J. Slingo (2001). The Diurnal Cycle in the Tropics. *Mon. Wea. Rev., 129*, 784–801.

Yin, J., J. D. Albertson, J. R. Rigby, and A. Porporato (2015). Land and atmospheric controls on initiation and intensity of moist convection: CAPE dynamics and LCL crossings. *Water Resources Research*, 51, 8476–8493.

Yin J, A. Molini, A. Porporato (2020). Impacts of Solar Intermittency on Future Photovoltaic Reliability. *Nat Communication* 11.

Zeng, D., X. Yuan, and J. K. Roundy, 2019: Effect of Teleconnected Land–Atmosphere Coupling on Northeast China Persistent Drought in Spring-Summer of 2017, *Journal of Climate*, 32, 7403-7420.